INTERNATIONAL CENTER FOR NUMERICAL METHODS IN ENGINEERING

On Isotropic Scalar Damage Models for the Numerical Analysis of Concrete Structures

R. Faria
J. Oliver
M.Cervera

Publication CIMNE Nº-198, December 2000

On Isotropic Scalar Damage Models for the Numerical Analysis of Concrete Structures

RUI FARIA

JAVIER OLIVER

MIGUEL CERVERA

SUMMARY

Within the framework of Continuum Damage Mechanics some isotropic scalar damage models for concrete are revisited, with emphasis on a recent one proposed by the authors. This scalar damage model is based on the assumption that a stress split is required to capture the unilateral behaviour exhibited by concrete when passing from tension to compression. Similar assumptions are pursued on many scalar damage models, yet with many differences being encountered on the strategies adopted for the implementation of such split, which sometimes is performed over the strain tensor. In this paper a discussion on the implications of those splits is conducted, as well as on the norms that define the elastic domain in the stress space. For the proposed damage model a strain-driven formalism is adopted, but the stress split is performed on the effective elastic stress tensor, which is shown to correspond to a split of the Cauchy stress tensor. This strategy improves the algorithmic efficiency as much as required for the seismic analysis of large-scale problems, and circumvents many of the drawbacks present in similar damage models. Besides, two scalar damage variables are introduced as internal variables, as well as an inelastic strain tensor. Efficiency of the proposed constitutive model is illustrated through numerical applications. Algorithmic implementation is also detailed.

Keywords: concrete, stress split, scalar norms, thermodynamics, damage variables, irreversible deformations.

1. INTRODUCTION

A large set of constitutive models for the modelling of concrete is presently available, namely the ones based on the theories of Hypo and Hyperelasticity, Plasticity, Fracture, Plastic-Fracture or Continuum Damage Mechanics. Based on the Thermodynamics of Irreversible Processes, Continuum Damage Mechanics provides a powerful and general framework for the derivation of consistent material models suitable for many engineering fields. Firstly introduced for creep-related problems[1], nowadays Damage Mechanics covers a broad range of applicability, for materials so different as metals, ceramics, rock and concrete[2-13]. Among the reasons for such a large acceptance, the versatility of the inherent Theory of Irreversible Processes can be pointed out, as well as its thermodynamic consistency.

In Section 2 a recent model proposed by the authors is presented. Supported on a strain-based formalism, the following basic features of concrete behaviour were selected as relevant to be accounted for in the constitutive model: (*i*) the rather different stress-strain envelopes observed under tension or under compression, (*ii*) the stiffness recovery upon loading reversal (visible when passing from tension to compression, or backwards), (*iii*) the concrete strength enhancement discernible under 2D or 3D compressive tests, when compared to the 1D compressive strength, and (*iv*) the inelastic deformations observable upon unloading.

The dissimilar behaviour exhibited by concrete under tension or under compression is an essential feature when dealing with cyclic actions. This peculiarity of concrete's behaviour, also exhibited by other geomaterials, is a consequence of the rather different strengths exhibited under tension or under compression, the first one associated to significant fragility, responsible for visible cracking. Therefore, under cyclic loading tensile cracking is usually the first evidence of nonlinearity, and consequently important changes in stiffness are observed when passing from tension to compression. To cope with this unilateral effect, clearly visible when reversing the sign of the external loading (as in earthquake motion), the constitutive model must be able, somehow, to distinguish tension from compression. An essential feature of the proposed model is that a split into tensile and compressive contributions will be introduced in the definition of the Helmholtz free energy. Two scalar damage variables are selected, each of them associated to the degradation mechanisms occurring under tensile or compressive stress conditions (assumed as independent).

The proposed model was devised to provide high algorithmic efficiency, a feature of primary importance when seismic analysis of large-scale concrete structures are envisaged. To account for this requisite a strain-driven formalism is adopted throughout, since the strain tensor is the first entity to be computed in standard displacement-based finite element codes. Typical disadvantages of classical strain-based splits – namely the inability to account for the strength enhancement in compression due to lateral confinement – are circumvented by defining the energy potential as a function of the effective elastic stress tensor, and not in terms of the strain tensor, the former a physically more relevant entity. This strategy preserves the advantages of a strain-driven formulation, since the effective stress tensor is itself a strain-based entity, and circumvents the drawbacks inherent to those formulations based on the final Cauchy stress tensor, which require an iterative procedure inside the constitutive model.

Close to the end of Section 2 the model capabilities are extended to account for irreversible deformations, and in order to clarify the implementation of the proposed model the most relevant algorithmic steps required for its coding will be presented. Some attention will be also devoted to the derivation of the inherent tangent matrix, but in order to avoid unnecessary detailing the most cumbersome operations are transferred to an Appendix, whereas in Section 2 only the most relevant aspects of the derivation will be presented.

To emphasise the implications arising from the different backgrounds in which are founded the proposed and some 'parent' scalar damage models, a comparative discussion is presented in Section 3, pointing out the major advantages and drawbacks of the corresponding formulations. The background of the proposed constitutive model was inspired in other concrete constitutive models founded on Damage Mechanics[12,14], although with important differences namely in what concerns the precise strategy pursued for the split, and the tensors that are involved in the definition of the energy potentials.

Section 4 is devoted to the validation of the proposed model through comparison of the corresponding numerical predictions with the experimental responses obtained for several structural applications.

A final Section with the most relevant conclusions closes the paper.

2. TWO SCALAR DAMAGE VARIABLES MODEL

2.1 Effective stress tensor

In the ensuing a basic entity, the rank-two *effective stress tensor*[5], is postulated as

$$\overline{\boldsymbol{\sigma}} = \boldsymbol{D}_0 : \boldsymbol{\varepsilon} \tag{1}$$

where $\boldsymbol{D}_0$ denotes the rank-four isotropic linear-elastic constitutive tensor and $\boldsymbol{\varepsilon}$ is the rank-two strain tensor. The effective stress tensor defined through equation (1) coincides with the definition of an elastic stress tensor, having considerable physical relevance since on a damaged material it corresponds to the stresses acting on the 'net' cross section, that is, excluding voids, cracks or any other imperfections, here looked as *damages*.

In order to account for the concrete unilateral effect, a split of the effective stress tensor $\overline{\boldsymbol{\sigma}}$ into tensile and compressive components, $\overline{\boldsymbol{\sigma}}^+$ and $\overline{\boldsymbol{\sigma}}^-$, is introduced, and performed according to[15]

$$\overline{\boldsymbol{\sigma}}^+ = \sum_i < \overline{\sigma}_i > \boldsymbol{p}_i \otimes \boldsymbol{p}_i \tag{2a}$$

$$\overline{\boldsymbol{\sigma}}^- = \overline{\boldsymbol{\sigma}} - \overline{\boldsymbol{\sigma}}^+ \tag{2b}$$

where $\overline{\sigma}_i$ refers the i-th principal stress of tensor $\overline{\boldsymbol{\sigma}}$ and $\boldsymbol{p}_i$ denotes the versor of the associated principal direction. The ramp function indicated by the Macaulay brackets $< \cdot >$ returns the value of the enclosed expression if positive, but sets a zero value if negative. As in equations (2), in the ensuing lines tensile and compressive entities will be pointed out through the using of indices (+) and (–), respectively.

2.2 Free energy potential

For a consistent derivation of a constitutive law a Helmholtz free energy potential with the form[15-17]

$$\psi\,(\boldsymbol{\varepsilon}, d^+, d^-) = (1-d^+)\,\psi_0^+(\boldsymbol{\varepsilon}) + (1-d^-)\,\psi_0^-(\boldsymbol{\varepsilon}) \tag{3}$$

is postulated, where ψ_0^+ and ψ_0^- are elastic free energies, defined according to

$$\psi_0^+(\boldsymbol{\varepsilon}) = 1/2\ \overline{\boldsymbol{\sigma}}^+ : \boldsymbol{D}_0^{-1} : \overline{\boldsymbol{\sigma}} = 1/2\ \overline{\boldsymbol{\sigma}}^+ : \boldsymbol{\varepsilon} \tag{4a}$$

$$\psi_0^-(\boldsymbol{\varepsilon}) = 1/2\ \overline{\boldsymbol{\sigma}}^- : \boldsymbol{D}_0^{-1} : \overline{\boldsymbol{\sigma}} = 1/2\ \overline{\boldsymbol{\sigma}}^- : \boldsymbol{\varepsilon} \tag{4b}$$

The set of internal variables is therefore constituted by the d^+ and d^- scalar damage variables, which correspond to the surface density of material defects, and range from 'zero' (for the virgin material) to 'one' (at collapse). These damage variables are directly linked to tensile and compressive deteriorations, herein after assumed as independent processes. Strain tensor $\boldsymbol{\varepsilon}$ is the only free variable admitted.

As demonstrated in Reference 17

$$\psi_0^+ \geq 0 \qquad\qquad \psi_0^- \geq 0 \tag{5}$$

and consequently, taking into consideration the intrinsic definition of damage,

$$0 \leq (d^+, d^-) \leq 1 \tag{6}$$

it is easy to demonstrate the positiveness of ψ:

$$\psi = (1-d^+)\,\psi_0^+ + (1-d^-)\,\psi_0^- \geq 0 \tag{7}$$

2.3 Constitutive equation

Since during a loading process non-negative energy dissipation has to be observed, thermodynamic consistency requires the Clausius-Duhem inequality to be satisfied, that is,

$$\dot{\gamma} = -\dot{\psi} + \boldsymbol{\sigma} : \dot{\boldsymbol{\varepsilon}} \geq 0 \tag{8}$$

From equation (3) it follows that

$$\dot{\psi} = \frac{\partial \psi}{\partial \boldsymbol{\varepsilon}} : \dot{\boldsymbol{\varepsilon}} - \psi_0^+ \dot{d}^+ - \psi_0^- \dot{d}^- \tag{9}$$

and consequently equation (8) assumes the form

$$\dot{\gamma} = \left(\boldsymbol{\sigma} - \frac{\partial \psi}{\partial \boldsymbol{\varepsilon}} \right) : \dot{\boldsymbol{\varepsilon}} + \psi_0^+ \dot{d}^+ + \psi_0^- \dot{d}^- \geq 0 \tag{10}$$

Pursuing standard reasonings, and since $\boldsymbol{\varepsilon}$ is a free variable, for the equation of dissipation to maintain its generality the expression within parenthesis should vanish, that is,

$$\boldsymbol{\sigma} = \frac{\partial \psi}{\partial \boldsymbol{\varepsilon}} \tag{11}$$

a Coleman's relation from which the constitutive law is derived. Due to the definition for the free energy potential expressed in (3), equation (11) leads to

$$\boldsymbol{\sigma} = (1-d^{+})\,\frac{\partial \psi_0^{+}}{\partial \boldsymbol{\varepsilon}} + (1-d^{-})\,\frac{\partial \psi_0^{-}}{\partial \boldsymbol{\varepsilon}} \tag{12}$$

Taking into consideration the equations (4), the linear dependency between $\overline{\boldsymbol{\sigma}}$ and $\boldsymbol{\varepsilon}$ expressed in (1), the stress split postulated in (2), and the fact that $\overline{\boldsymbol{\sigma}}^{+}$ and $\overline{\boldsymbol{\sigma}}^{-}$ are degree-one homogeneous functions of $\boldsymbol{\varepsilon}$, owing to Euler's theorem in Reference 17 it is shown that

$$\frac{\partial \psi_0^{+}}{\partial \boldsymbol{\varepsilon}} = \overline{\boldsymbol{\sigma}}^{+} \qquad\qquad \frac{\partial \psi_0^{-}}{\partial \boldsymbol{\varepsilon}} = \overline{\boldsymbol{\sigma}}^{-} \tag{13}$$

Substituting in equation (12) a final form for the constitutive law is then accessible, leading to a rather intuitive expression for the $\boldsymbol{\sigma}$ Cauchy stress tensor:

$$\boldsymbol{\sigma} = (1-d^{+})\,\overline{\boldsymbol{\sigma}}^{+} + (1-d^{-})\,\overline{\boldsymbol{\sigma}}^{-} \tag{14}$$

Remark 1. Due to the isotropy inherent to the scalar damage variables d^{+} and d^{-} and to the format of the present constitutive law, equation (14) points out that a split of tensor $\boldsymbol{\sigma}$ into tensile and compressive tensors $\boldsymbol{\sigma}^{+}$ and $\boldsymbol{\sigma}^{-}$ is implicit in the present formulation, that is,

$$\boldsymbol{\sigma}^{+} = (1-d^{+})\,\overline{\boldsymbol{\sigma}}^{+} \qquad\qquad \boldsymbol{\sigma}^{-} = (1-d^{-})\,\overline{\boldsymbol{\sigma}}^{-} \tag{15}$$

This relevant property emphasises that the adopted split of the effective stress tensor leads in fact to a related dual split of the Cauchy stress tensor. □

2.4 Elastic domain: damage criteria

Analogously to the *equivalent strain* postulated by Simo and Ju[18], let us define the dual concept of *equivalent stress*, a scalar positive norm that allows identifying 'loading', 'unloading' or 'reloading' situations. Since a clear distinction between tension and compression is assumed throughout based on the stress split defined in (2), a tensile equivalent stress τ_{σ}^{+} and a compressive equivalent stress τ_{σ}^{-} are postulated according to the forms

$$\tau_{\boldsymbol{\sigma}}^{+} = \sqrt{\boldsymbol{\sigma}^{+} : \boldsymbol{\Lambda}^{+} : \boldsymbol{\sigma}^{+}} \qquad\qquad \tau_{\boldsymbol{\sigma}}^{-} = \sqrt{\boldsymbol{\sigma}^{-} : \boldsymbol{\Lambda}^{-} : \boldsymbol{\sigma}^{-}} \tag{16}$$

where $\boldsymbol{\Lambda}^{\pm}$ are non-dimensional fourth-order metric tensors that define the shape of the damage bounding surfaces. In principle the one for tension, $\boldsymbol{\Lambda}^{+}$, is different from the

one for compression, $\boldsymbol{\Lambda}^-$, but both should be isotropic and positive definite, features that can be accomplished by adopting definitions like

$$\boldsymbol{\Lambda}^{\pm} = (1+\gamma^{\pm})\,\boldsymbol{I} - \gamma^{\pm}\,\mathbf{1}\otimes\mathbf{1} \tag{17}$$

where $\boldsymbol{I}$ and $\mathbf{1}$ are the rank-four and rank-two identity tensors. Parameters $\gamma^{\pm}$, which can be defined separately for tension and for compression, are devised to reproduce the equibiaxial/uniaxial strength ratios typical in concrete. They should be such that $\gamma^{\pm} \in [0, 1[$.

Calling for the stress norms defined in (16), two damage criteria $g^{\pm}$ in terms of the Cauchy stress tensors are introduced

$$g^+(\boldsymbol{\sigma}^+, q^+) = \tau^+_{\boldsymbol{\sigma}} - q^+ \leq 0 \tag{18a}$$

$$g^-(\boldsymbol{\sigma}^-, q^-) = \tau^-_{\boldsymbol{\sigma}} - q^- \leq 0 \tag{18b}$$

where $q^{\pm}$ are current thresholds that control the size of the damage surfaces, therefore playing the role of hardening-like internal variables. Consequently, and previously to the onset of damage, $q^{\pm}$ would have to be set equal to $q^{\pm}_0$, the initial values of such internal variables corresponding to the initial elastic domain. At any time the elastic domain defined by the criteria expressed in (18) is therefore the intersection

$$\mathrm{E}_{\boldsymbol{\sigma}} = \mathrm{E}^+_{\boldsymbol{\sigma}} \cap \mathrm{E}^-_{\boldsymbol{\sigma}} \tag{19}$$

with

$$\mathrm{E}^+_{\boldsymbol{\sigma}} = \left\{\boldsymbol{\sigma};\ g^+(\boldsymbol{\sigma}^+, q^+) < 0\right\} \qquad \mathrm{E}^-_{\boldsymbol{\sigma}} = \left\{\boldsymbol{\sigma};\ g^-(\boldsymbol{\sigma}^-, q^-) < 0\right\} \tag{20}$$

Figure 1 reproduces a characteristic configuration of the 2D initial elastic domain obtained in the present model[†]: in pure tension a rounded Rankine-type criterion is obtained by setting $\gamma^+ = 0.0$, whereas in pure compression a realistic equibiaxial/uniaxial strength ratio equal to 1.15 is obtained by adopting $\gamma^- = 0.622$. The overall agreement of this elastic domain with the one inferred form the experimental results due to Kupfer *et al.*[19] is fairly good, either in pure tension or in pure compression, or even in tension-compression situations.

[†] In this figure f^-_0 denotes the stress which defines the onset of damage in 1D compression.

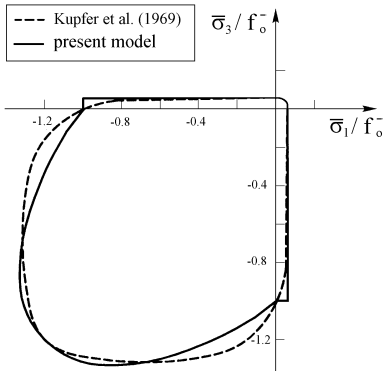

Figure 1. Initial 2D elastic domain.

2.5 Evolution of the damage variables

Let us assume that the damage variables are computed in accordance to

$$d^{\pm}(r^{\pm}) = 1 - \frac{q^{\pm}(r^{\pm})}{r^{\pm}} \tag{21}$$

where the hardening/softening thresholds $q^{\pm}$ are positive functions of some internal variables $r^{\pm}$, which in turn obey the kinematics

$$\dot{r}^{\pm} = \lambda^{\pm} \tag{22}$$

with $\lambda^{\pm} \geq 0$ being damage multipliers which will participate in the Kuhn-Tucker conditions. Through substitution of equations (16) in (18), owing to the split of tensor $\boldsymbol{\sigma}$ expressed in equation (15) and also to

$$q^{\pm}(r^{\pm}) = (1-d^{\pm})\, r^{\pm} \tag{23}$$

that arises from equation (21), it is worth noting that the criteria expressed in equations (18) are equivalent to

$$\bar{g}^{\pm}(\bar{\tau}^{\pm}, r^{\pm}) = \bar{\tau}^{\pm} - r^{\pm} \leq 0 \tag{24}$$

where

$$\bar{\tau}^{\pm} = \sqrt{\bar{\boldsymbol{\sigma}}^{\pm} : \boldsymbol{\Lambda}^{\pm} : \bar{\boldsymbol{\sigma}}^{\pm}} \tag{25}$$

Since the effective stress tensor is a strain-driven entity, the Kuhn-Tucker relations will be applied to the criteria expressed in the latter format (24), that is,

$$\bar{g}^{\pm} \leq 0 \qquad \lambda^{\pm} \geq 0 \qquad \lambda^{\pm}\, \bar{g}^{\pm} = 0 \tag{26}$$

Introducing the persistency condition it reads

$$\lambda^{\pm}\ \dot{\bar{g}}^{\pm}\ =\ 0 \tag{27}$$

and consequently for loading conditions one gets

$$\dot{\bar{g}}^{\pm}\ =\ 0 \qquad\qquad \dot{\bar{\tau}}^{\pm}\ =\ \dot{r}^{\pm}\ \geq\ 0 \tag{28}$$

Integrating for a generic instant *t*, in view of this equation the following conclusion arises

$$r_t^{\pm}\ =\ \max\ \left\{ r_0^{\pm}\,,\ \ \max_{s\,\in\,[0,\,t]}\,(\bar{\tau}^{\pm})_s \right\} \tag{29}$$

where $r_0^{\pm}$ are the thresholds that bound the initial linear-elastic domain; according to equation (23) it results

$$r_0^{\pm}\ =\ q_0^{\pm} \tag{30}$$

since $d^{\pm}\big|_{t=0}\ =\ 0$.

2.6 Dissipation

Owing to the non-negativeness of ψ_0^{+} and ψ_0^{-}, from equation (10) it can be inferred that for the dissipation

$$\dot{\gamma}\ =\ \psi_0^{+}\ \dot{d}^{+}\ +\ \psi_0^{-}\ \dot{d}^{-} \tag{31}$$

to satisfy the Clausius-Duhem inequality it suffices that

$$\dot{d}^{\pm}\ \geq\ 0 \tag{32}$$

These inequalities fix a classical condition on the rate evolution of the damage variables, or equivalently, it introduces the thermodynamic requirement that thresholds $q^{\pm}$ would have to satisfy, due to the links between the two entities expressed in equation (21):

$$\dot{d}^{\pm}\ =\ \left(-\frac{1}{r^{\pm}}\,\frac{\partial\, q^{\pm}}{\partial\, r^{\pm}}\ +\ \frac{q^{\pm}}{(r^{\pm})^{2}} \right) \dot{r}^{\pm}\ \geq\ 0 \tag{33}$$

Accounting to the conclusion expressed in equation (28), that is, $\dot{r}^{\pm} \geq 0$, condition (33) demands also the non-negativeness of the expression within brackets, and consequently

$$\frac{q^{\pm}}{r^{\pm}}\ \geq\ \frac{\partial\, q^{\pm}}{\partial\, r^{\pm}}\ =\ \mathrm{H}^{\pm} \tag{34}$$

where $\mathrm{H}^{\pm}$ may be looked as a hardening/softening parameter.

Remark 2. According to equations (6) and (23) condition $q^{\pm}/r^{\pm} \leq 1$ has to be satisfied, which combined with equation (34) leads to the conclusion that $\mathrm{H}^{\pm} \leq q^{\pm}/r^{\pm} \leq 1$. As depicted in Figure 2 this condition is trivially satisfied by the hardening/softening laws exhibited by the most relevant materials commonly used in engineering, and namely by the concrete. □

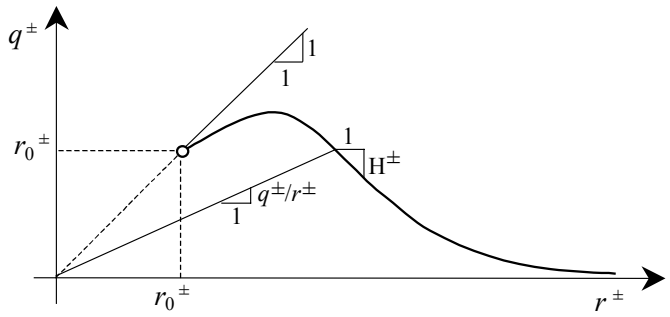

Figure 2. Hardening/softening condition.

2.7 Updating of the damage variables

From equation (29) it becomes clear that the updating of the internal variables $r^{\pm}$ constitutes an easy task, since only the maximum $\bar{\tau}^{\pm}$ need to be retained. Consequently the damage variables can be updated quite easily, because owing to equation (21) they are explicit functions of thresholds $r^{\pm}$, provided that suitable formats are attributed to functions $q^{\pm}(r^{\pm})$. The selection of these functions will determine the specific damage evolutions to be considered, and consequently some care must be devoted to this subject, so that realistic kinematics for $d^{\pm}$ are included in the numerical model. Anyway, the change from one particular set of evolution laws to a different one does not put any special problem, thus enabling the constitutive model to have substantial updating versatility.

In the present work the following evolution rules are adopted, which fulfil the requirements expressed in (34):

$$q^{+}(r^{+}) = r_0^{+}\, e^{A\,(1 - r^{+}/r_0^{+})} \qquad \text{if } r^{+} \geq r_0^{+} \qquad (35a)$$

$$q^{-}(r^{-}) = r_0^{-}\,(1-B) + r^{-}\,B\, e^{C\,(1 - r^{-}/r_0^{-})} \qquad \text{if } r^{-} \geq r_0^{-} \qquad (35b)$$

For a 1D tensile test equation (35*a*) provides a softening branch that is asymptotic to the strain axis. With such an evolution law[20] a finite area is retained between the stress-strain curve and the strain axis, which has to be appropriately related to the concrete fracture energy so as to satisfy requirements of mesh-objectivity, an issue that can be solved by introducing a characteristic length l depending on the spatial discretization[21]. Consequently the unique parameter A involved in equation (35*a*) is computed by equating the concrete fracture energy G per unit of the characteristic length to the time integral of dissipation on a 1D tensile test, rendering[20]

$$A = \left(\frac{G\,E}{l\,(\mathrm{f}_0^+)^2} - \frac{1}{2} \right)^{-1} \geq 0 \tag{36}$$

where f_0^+ denotes the concrete tensile strength and E is the Young's modulus.

Equation (35*b*) allows reproducing the hardening in concrete under compression, as well as the softening which characterises the post-peak behaviour. Definition of the two parameters B and C is required, usually by imposing the numerical curve to pass in two selected points of a curve from a 1D compressive test.

2.8 Extension to account for inelastic strains

- *Evolution law*

Rather small modifications need to be introduced in the formulation of the proposed model to account for the inelastic strains that are observed in concrete upon unloading. Let us call for the additive rule $\boldsymbol{\varepsilon} = \boldsymbol{\varepsilon}^e + \boldsymbol{\varepsilon}^i$, where $\boldsymbol{\varepsilon}^e$ and $\boldsymbol{\varepsilon}^i$ stand for the elastic and inelastic strain tensors, respectively.

By assuming that the rate of the inelastic strains $\boldsymbol{\varepsilon}^i$ is forced to occur in the same direction of the elastic strain tensor we postulate the following law

$$\dot{\boldsymbol{\varepsilon}}^i = \dot{b}\,\boldsymbol{\varepsilon}^e \tag{37}$$

with

$$\dot{b} = \beta E\, H(\dot{d}^-)\, \frac{<\overline{\boldsymbol{\sigma}} : \dot{\boldsymbol{\varepsilon}}>}{\overline{\boldsymbol{\sigma}} : \overline{\boldsymbol{\sigma}}} \geq 0 \tag{38}$$

being a non-negative scalar, where $\beta \geq 0$ is a material parameter that controls the intensity of the inelastic deformation and $H(\dot{d}^-)$ is the Heaviside function computed for the damage rate in compression.

This format for the inelastic strain evolution is somehow inspired on the Generalised Plasticity Theory†, since the typical ingredients of such approach[22] can be identified in equations (37-38): *(i)* the dependency of the irreversible strain change on the strain rate $\dot{\boldsymbol{\varepsilon}}$ and *(ii)* the explicit inclusion of the loading or unloading direction via factor $H(\dot{d}^-)$. This directional loading factor hinders the inelastic straining during unloading or before the damage threshold being attained in a compressive test. Additionally, it also precludes the evolution of the irreversible strains in a pure tensile test, a simplification adopted here to reduce the complexity of the approach, since the present constitutive model is mainly intended for large time consuming analysis, and only an overall representation of the irreversible straining effect is intended.

- *Free energy potential and dissipation*

With the inclusion of the irreversible strain tensor $\boldsymbol{\varepsilon}^i$ the effective stress tensor is redefined as a function of the elastic strain tensor $\boldsymbol{\varepsilon}^e$, that is,

$$\overline{\boldsymbol{\sigma}} \;=\; \boldsymbol{D}_0 : \boldsymbol{\varepsilon}^e \;=\; \boldsymbol{D}_0 : (\boldsymbol{\varepsilon} - \boldsymbol{\varepsilon}^i) \tag{39}$$

a postulate that replaces equation (1).

Accordingly the elastic free energies expressed in equations (4) should be rewritten as

$$\psi_0^+(\boldsymbol{\varepsilon}^e) \;=\; 1/2\;\; \overline{\boldsymbol{\sigma}}^+ : \boldsymbol{\varepsilon}^e \qquad\qquad \psi_0^-(\boldsymbol{\varepsilon}^e) \;=\; 1/2\;\; \overline{\boldsymbol{\sigma}}^- : \boldsymbol{\varepsilon}^e \tag{40}$$

and the free energy potential (3) is thereafter replaced by the following one

$$\psi\;(\boldsymbol{\varepsilon},\, \boldsymbol{\varepsilon}^i,\, d^+,\, d^-) \;=\; (1-d^+)\;\psi_0^+(\boldsymbol{\varepsilon}-\boldsymbol{\varepsilon}^i) \;+\; (1-d^-)\;\psi_0^-(\boldsymbol{\varepsilon}-\boldsymbol{\varepsilon}^i) \;\;\geq\; 0 \tag{41}$$

As demonstrated in Reference 17 the constitutive law defined through equation (14) is kept unchanged, since according to the chain rule it is possible to rewrite equation (11) as

$$\boldsymbol{\sigma} \;=\; \frac{\partial \psi}{\partial \boldsymbol{\varepsilon}} \;=\; \frac{\partial \psi}{\partial \boldsymbol{\varepsilon}^e} \;=\; (1-d^+)\,\frac{\partial \psi_0^+}{\partial \boldsymbol{\varepsilon}^e} \;+\; (1-d^-)\,\frac{\partial \psi_0^-}{\partial \boldsymbol{\varepsilon}^e} \tag{42}$$

and

$$\frac{\partial \psi_0^+}{\partial \boldsymbol{\varepsilon}^e} \;=\; \overline{\boldsymbol{\sigma}}^+ \qquad\qquad \frac{\partial \psi_0^-}{\partial \boldsymbol{\varepsilon}^e} \;=\; \overline{\boldsymbol{\sigma}}^- \tag{43}$$

---

† According to the above definitions $\boldsymbol{\varepsilon}^e$ may be looked as the 'direction of inelastic flow' and $\dot{b}$ as the 'inelastic multiplier'.

In what concerns the dissipation, as a new internal variable $\boldsymbol{\varepsilon}^i$ is introduced in (41) the following new term has to be added to equation (31):

$$-\frac{\partial \psi}{\partial \boldsymbol{\varepsilon}^i} : \dot{\boldsymbol{\varepsilon}}^i \tag{44}$$

Since

$$\frac{\partial \psi}{\partial \boldsymbol{\varepsilon}^i} = -\frac{\partial \psi}{\partial \boldsymbol{\varepsilon}^e} = -\left[(1-d^+)\,\overline{\boldsymbol{\sigma}}^+ + (1-d^-)\,\overline{\boldsymbol{\sigma}}^-\right] \tag{45}$$

substitution of this result and equation (37) into equation (44) leads to

$$-\frac{\partial \psi}{\partial \boldsymbol{\varepsilon}^i} : \dot{\boldsymbol{\varepsilon}}^i = 2\,\dot{b}\,\psi \tag{46}$$

Taking into consideration that $\psi \geq 0$ (see equation (41)) this additional contribution to dissipation will be non-negative if $\dot{b} \geq 0$, a requirement that is systematically fulfilled owing to the particular format adopted in equations (37-38) for the rate evolution of the irreversible strain tensor, where the Macaulay brackets play an essential role. Consequently, condition of dissipation $\dot{\gamma} \geq 0$ is satisfied.

- *Integration*

By differentiating equation (39) with respect to time, owing to equations (37-38) it results:

$$\dot{\overline{\boldsymbol{\sigma}}} = \boldsymbol{D}_0 : \dot{\boldsymbol{\varepsilon}} - \beta\, E\, H(\dot{d}^-) < \overline{\boldsymbol{\sigma}} : \dot{\boldsymbol{\varepsilon}} > \frac{\overline{\boldsymbol{\sigma}}}{\overline{\boldsymbol{\sigma}} : \overline{\boldsymbol{\sigma}}} \tag{47}$$

If a backward-Euler time discretization scheme is adopted, with $(\cdot)_n$ and $(\cdot)_{n+1}$ denoting entities pertaining to consecutive time steps and $\Delta\boldsymbol{\varepsilon}$ referring to the inherent increment of $\boldsymbol{\varepsilon}$, one gets

$$\overline{\boldsymbol{\sigma}}_{n+1} = \overline{\boldsymbol{\sigma}}_n + \boldsymbol{D}_0 : \Delta\boldsymbol{\varepsilon} - \beta\, E\, H(\dot{d}^-_{n+1}) < \overline{\boldsymbol{\sigma}}_{n+1} : \Delta\boldsymbol{\varepsilon} > \frac{\overline{\boldsymbol{\sigma}}_{n+1}}{\overline{\boldsymbol{\sigma}}_{n+1} : \overline{\boldsymbol{\sigma}}_{n+1}} \tag{48}$$

Defining

$$\overline{\boldsymbol{\sigma}}^{trial}_{n+1} = \overline{\boldsymbol{\sigma}}_n + \boldsymbol{D}_0 : \Delta\boldsymbol{\varepsilon} \tag{49}$$

it is possible to attribute the following form[17] to equation (48)

$$\overline{\boldsymbol{\sigma}}_{n+1} = \alpha\, \overline{\boldsymbol{\sigma}}^{trial}_{n+1} \tag{50}$$

where

$$\alpha \;=\; 1 \;-\; \beta\, E\, H(\dot{d}^{-}_{n+1})\; \frac{<\overline{\boldsymbol{\sigma}}^{trial}_{n+1} : \Delta\boldsymbol{\varepsilon}>}{\overline{\boldsymbol{\sigma}}^{trial}_{n+1} : \overline{\boldsymbol{\sigma}}^{trial}_{n+1}} \tag{51}$$

Since $\Delta\boldsymbol{\varepsilon}$ and $\overline{\boldsymbol{\sigma}}^{trial}_{n+1}$ are explicit in terms of the strains at step n+1, the effective stress tensor ends being a strain-based entity, which can be updated according to the 'radial return' algorithm reproduced in equations (50-51): tensor $\overline{\boldsymbol{\sigma}}^{trial}_{n+1}$ is a trial predictor, through which the final effective stress tensor can be obtained once computed the scale factor α. The 0/1 discontinuity in equation (51) due to the Heaviside function requires a maximum of two iterations to be performed, and consequently high algorithmic efficiency is guaranteed with the proposed format for the inelastic strain evolution.

2.9 Algorithm

Owing to the strain-driven formalism of the proposed constitutive model, and to the fact of $\boldsymbol{\varepsilon}$ being fully determined at the beginning of each step of a displacement-based finite element algorithm, its code implementation is quite straightforward, as illustrated in Table 1.

Table 1. Algorithm for the two scalar damage variables model

Step *n*=0:

(i) Set $r^{+}_{n} = r^{+}_{0}$, $r^{-}_{n} = r^{-}_{0}$, $d^{+}_{n} = 0$ and $d^{-}_{n} = 0$.

Step *n*+1:

(ii) Evaluate $\boldsymbol{\varepsilon}_{n+1}$ and $\Delta\boldsymbol{\varepsilon}$. Compute $\overline{\boldsymbol{\sigma}}_{n+1}$ according to equations (49-51).

(iii) Split $\overline{\boldsymbol{\sigma}}_{n+1}$ into $\overline{\boldsymbol{\sigma}}^{+}_{n+1}$ and $\overline{\boldsymbol{\sigma}}^{-}_{n+1}$ according to equations (2).

(iv) Compute $\overline{\tau}^{+}_{n+1}$ and $\overline{\tau}^{-}_{n+1}$ according to equations (25).

(v) If $\overline{\tau}^{\pm}_{n+1} > r^{\pm}_{n}$ update thresholds: $r^{\pm}_{n+1} = \max\left\{r^{\pm}_{n},\ \overline{\tau}^{\pm}_{n+1}\right\}$.
Update damage variables $d^{\pm}_{n+1} = 1 - q^{\pm}(r^{\pm}_{n+1})/r^{\pm}_{n+1}$ according to equations (21,35) (or equivalent ones).

(vi) Compute the Cauchy stress tensor

$$\boldsymbol{\sigma}_{n+1} \;=\; \left(1-d^{+}_{n+1}\right)\overline{\boldsymbol{\sigma}}^{+}_{n+1} \;+\; \left(1-d^{-}_{n+1}\right)\overline{\boldsymbol{\sigma}}^{-}_{n+1} \qquad \text{EXIT.}$$

2.10 Performance in 1D cyclic conditions

Figure 3 depicts the typical performance of the constitutive model during a 1D tension-compression cyclic test. The ability of the inelastic-damage model to reproduce the softening behaviour under tension becomes evident, as well as the hardening and softening under compression. During the incursions into the tensile regimen the irreversible strains are prevented to increase, as evidenced during the first tensile unloading (line B-O), but accumulation of irreversible deformations occurs during increased loading in compression. Stiffness recovery is also clearly detected during paths B-O-C, D-E-F or G-E-D, a unilateral effect easily captured by the two different damage variables adopted in the constitutive model.

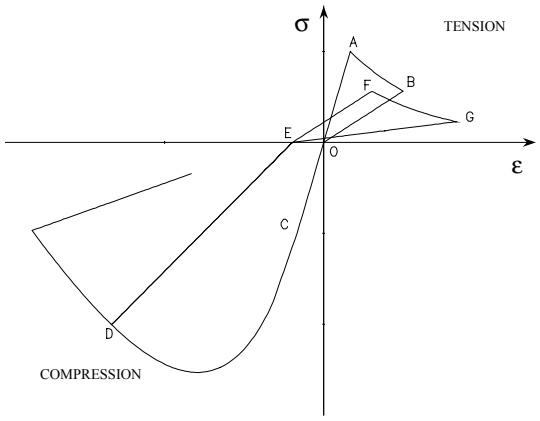

Figure 3. Cyclic behaviour during a 1D test.

2.11 Tangent matrix

Derivation of a consistent tangent matrix for the proposed model demands the constitutive law (14) to be differentiated with respect to time:

$$\dot{\boldsymbol{\sigma}} = (1-d^{+})\,\dot{\overline{\boldsymbol{\sigma}}}^{+} + (1-d^{-})\,\dot{\overline{\boldsymbol{\sigma}}}^{-} - \overline{\boldsymbol{\sigma}}^{+}\,\dot{d}^{+} - \overline{\boldsymbol{\sigma}}^{-}\,\dot{d}^{-} \tag{52}$$

In equation (47) a time differentiation of tensor $\overline{\boldsymbol{\sigma}}$ was already presented. Rewriting it on a more suitable format as

$$\dot{\overline{\boldsymbol{\sigma}}} = \boldsymbol{D}^{i} : \dot{\boldsymbol{\varepsilon}} \tag{53}$$

little mathematical handling is required to conclude that $\boldsymbol{D}^{i}$ is the following symmetric matrix:

$$\boldsymbol{D}^{i} = \boldsymbol{D}_{0} - \beta\, E\, H(\dot{d}^{-})\, H(\overline{\boldsymbol{\sigma}} : d\boldsymbol{\varepsilon})\, \frac{\overline{\boldsymbol{\sigma}} \otimes \overline{\boldsymbol{\sigma}}}{\overline{\boldsymbol{\sigma}} : \overline{\boldsymbol{\sigma}}} \tag{54}$$

In spite of the intrinsic simplicity of the split postulated in equations (2), which expresses $\overline{\boldsymbol{\sigma}}^{\pm}$ as functions of the eigenvalues and eigenvectors of $\overline{\boldsymbol{\sigma}}$, quite more complex operations are required to express $\dot{\overline{\boldsymbol{\sigma}}}^{+}$ as a function of $\dot{\overline{\boldsymbol{\sigma}}}$. In the Appendix an operator $\mathbf{P}$ such that

$$\dot{\overline{\boldsymbol{\sigma}}}^{+} = \mathbf{P} : \dot{\overline{\boldsymbol{\sigma}}} = \mathbf{P} : \boldsymbol{D}^{i} : \dot{\boldsymbol{\varepsilon}} \tag{55a}$$

$$\dot{\overline{\boldsymbol{\sigma}}}^{-} = (\boldsymbol{I} - \mathbf{P}) : \dot{\overline{\boldsymbol{\sigma}}} = (\boldsymbol{I} - \mathbf{P}) : \boldsymbol{D}^{i} : \dot{\boldsymbol{\varepsilon}} \tag{55b}$$

is presented. Here it suffices to express $\mathbf{P}$ as

$$\mathbf{P} = \sum_{i=1}^{3} H(\overline{\sigma}_i)\, \boldsymbol{P}^{ii} \otimes \boldsymbol{P}^{ii} + 2 \sum_{\substack{i,j=1 \\ j>i}}^{3} \frac{<\overline{\sigma}_i> - <\overline{\sigma}_j>}{\overline{\sigma}_i - \overline{\sigma}_j}\, \boldsymbol{P}^{ij} \otimes \boldsymbol{P}^{ij} \tag{56}$$

where

$$\boldsymbol{P}^{ij} = \boldsymbol{P}^{ji} = \frac{1}{2}\left(\boldsymbol{p}_i \otimes \boldsymbol{p}_j + \boldsymbol{p}_j \otimes \boldsymbol{p}_i\right) = \operatorname{symm}\left(\boldsymbol{p}_i \otimes \boldsymbol{p}_j\right) \tag{57}$$

Therefore, for complete clarification of equation (52) it is only required to write explicitly the rate evolutions for $\dot{d}^{\pm}$ (under loading conditions). In compacted form equation (33) can be expressed as

$$\dot{d}^{\pm} = h^{\pm}\, \dot{r}^{\pm} \tag{58}$$

with

$$h^{\pm} = -\frac{1}{r^{\pm}} \mathrm{H}^{\pm} + \frac{q^{\pm}}{(r^{\pm})^2} \tag{59}$$

Owing to equation (28) $\dot{r}^{\pm} = \dot{\overline{\tau}}^{\pm}$. Consequently, and according to equations (25), it follows

$$\dot{r}^{+} = \frac{1}{\overline{\tau}^{+}}\, \overline{\boldsymbol{\sigma}}^{+} : \boldsymbol{\Lambda}^{+} : \dot{\overline{\boldsymbol{\sigma}}}^{+} = \frac{1}{\overline{\tau}^{+}}\, \overline{\boldsymbol{\sigma}}^{+} : \boldsymbol{\Lambda}^{+} : \mathbf{P} : \boldsymbol{D}^{i} : \dot{\boldsymbol{\varepsilon}} \tag{60a}$$

$$\dot{r}^{-} = \frac{1}{\overline{\tau}^{-}}\, \overline{\boldsymbol{\sigma}}^{-} : \boldsymbol{\Lambda}^{-} : \dot{\overline{\boldsymbol{\sigma}}}^{-} = \frac{1}{\overline{\tau}^{-}}\, \overline{\boldsymbol{\sigma}}^{-} : \boldsymbol{\Lambda}^{-} : \left(\boldsymbol{I} - \mathbf{P}\right) : \boldsymbol{D}^{i} : \dot{\boldsymbol{\varepsilon}} \tag{60b}$$

Introducing these results in equation (58), which in turn is used in (52) jointly with equations (55), one gets

$$\dot{\boldsymbol{\sigma}} = \boldsymbol{D}_{tan} : \dot{\boldsymbol{\varepsilon}} \tag{61}$$

where for the tangent matrix $\boldsymbol{D}_{tan}$ the following expression applies:

$$\boldsymbol{D}_{tan} = \left\{ \left((1-d^{+})\,\boldsymbol{I} \; - \; \frac{h^{+}}{\overline{\tau}^{+}} (\overline{\boldsymbol{\sigma}}^{+} \otimes \overline{\boldsymbol{\sigma}}^{+}) : \boldsymbol{\Lambda}^{+} \right) : \mathbf{P} \; + \right.$$

$$\left. + \left((1-d^{-})\,\boldsymbol{I} \; - \; \frac{h^{-}}{\overline{\tau}^{-}} (\overline{\boldsymbol{\sigma}}^{-} \otimes \overline{\boldsymbol{\sigma}}^{-}) : \boldsymbol{\Lambda}^{-} \right) : (\boldsymbol{I} - \mathbf{P}) \right\} : \boldsymbol{D}^{i} \qquad (62)$$

This operator is non-symmetric under general conditions, and it applies whilst 'loading' conditions are observed. If 'unloading' occurs in tension or in compression the evolution of the corresponding damage variable is null, and consequently it suffices to take $h^{+}=0$ or $h^{-}=0$ in (62). If 'unloading' occurs in compression it should also be considered that $\boldsymbol{D}^{i}=\boldsymbol{D}_{0}$.

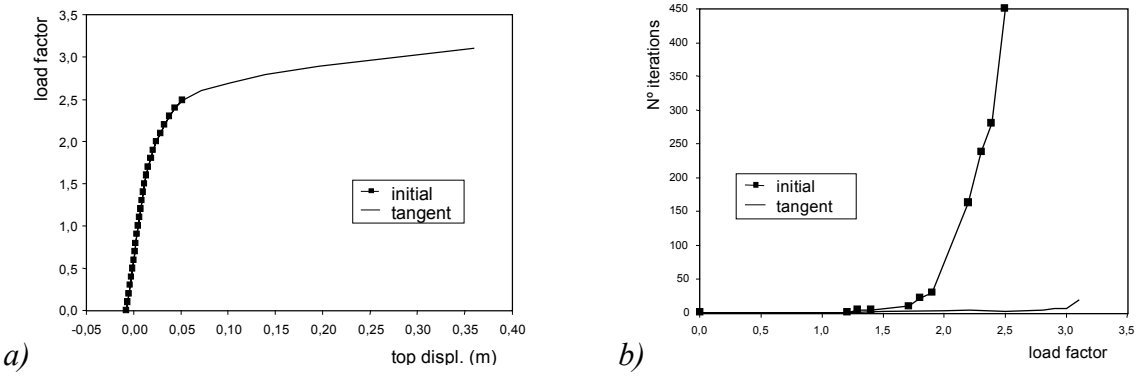

a) *b)*

Figure 4. Performance of the tangent matrix on the analysis of Koyna dam.

Figure 4 illustrates the performance of a Newton-Raphson algorithm when the proposed constitutive model is used jointly with the tangent matrix here derived. It concerns the numerical simulation of a scenario for the gravity Koyna dam, where the hydrostatic impulse is monotonically increased by a load factor up to failure. Since the simulation itself is somewhat irrelevant for the present illustrative purposes (further details can be found in Reference 16), we will focus solely on the comparison of the numerical results obtained with the tangent matrix or by using a modified Newton-Raphson algorithm supported on the initial elastic stiffness matrix. Figure 4*a* depicts the evolution of the load factor with the horizontal displacement at the crest of the dam, and points out the inability from the 'initial' strategy to provide solutions for load factors greater than 2.5, contrarily to the 'tangent' one which steps considerably further close to collapse. The quadratic convergence from the 'tangent' algorithm

provides also a drastic reduction on the number of iterations required for convergence, in comparison with the 'initial' one, as reproduced in Figure 4*b*.

3. COMPARATIVE DISCUSSION

3.1 Overview

The damage model formulation detailed in Section 2 is based on a split of the effective stress tensor $\overline{\boldsymbol{\sigma}}$ into tensile and compressive stress tensors, which associated with the scalar damage variables $d^{\pm}$ play an essential role in the definition of the free energy potential. Moreover, tensors $\overline{\boldsymbol{\sigma}}^{+}$ and $\overline{\boldsymbol{\sigma}}^{-}$ are mapped onto a 1D domain via the scalar norms $\overline{\tau}^{\pm}$, equivalent stresses which participate in the definition of the two damage criteria introduced in equation (24).

Therefore, both the split and the 'structure' of the free energy potential, and even the norms and the damage criteria resemble the features of other models based on Continuum Damage Mechanics. For instance, Reference 23 a similar split is documented, yet performed over the strain tensor, and in Reference 12 a split of the strain tensor into $\boldsymbol{\varepsilon}^{\pm}$ is also referred, associated to different variants of Mazars' models.

Concerning the damage criteria, the format adopted here is clearly inspired on the original one proposed in Reference 18, but extended to account for the split of the effective stress tensor.

With reference to the scalar norms $\overline{\tau}^{\pm}$, in the above references definitions similar to the ones postulated here are encountered. In fact many different norms have been proposed in the literature[12,18,20,24], associated to several damage criteria. A crucial distinction between those norms and damage criteria concerns the basic entity on which they are based, and at least two families can be identified: *(i)* the strain-based ones and *(ii)* the stress-based ones. Apparently this may be thought to reflect the different appraisals concerning the basic mechanisms which guide the initiation and progression of damage in concrete, particularly the one associated to cracking, where interpretations linking this phenomenon to lateral expansion (volume increase) or to tensile stresses are commonly encountered. These interpretations depend mostly on the level under which the model approximation is introduced, since under a microscopic or intermediate level cracking in the cement paste is frequently attributed to tensile stresses that form due to bridging between the aggregates, whereas under a macroscopic standpoint, and for

instance during a uniaxial compressive test, the visible cracking is not easily associated to tensile loading, and consequently sometimes it is associated with lateral positive straining[†].

Therefore, and since some common features exist between the model described in Section 2 and the 'parent' ones, a pertinent doubt concerning the real differences between them may arise in the reader's mind. In spite of several similarities, some relevant discrepancies exist between the many formulations just mentioned, with implications in the code implementation and in the computational efficiency.

3.2 Free energy potential

The free energy potential assumed in the present paper (equation (3)) may be compared to the one in Reference 12, whose form is:

$$\psi = \frac{1}{2(1-d^{+})}\,\boldsymbol{\sigma}^{+} : \boldsymbol{D}_0^{-1} : \boldsymbol{\sigma}^{+} + \frac{1}{2(1-d^{-})}\,\boldsymbol{\sigma}^{-} : \boldsymbol{D}_0^{-1} : \boldsymbol{\sigma}^{-} \tag{63}$$

A fundamental particularity that can detected in this definition is that the Cauchy stress tensor $\boldsymbol{\sigma}$ is mobilised, whilst in equation (3) we have adopted the effective stress tensor $\overline{\boldsymbol{\sigma}}$. Since $\boldsymbol{\sigma}$ is the stress tensor to be evaluated, in (63) an implicit formulation is therefore involved, which obviously requires an iterative procedure to be implemented within the constitutive model. In (3) the constitutive model is intentionally written in terms of the effective stress tensor (or their split components), a rather more explicit entity due to its strain-driven background. Anyway, and as emphasised in (15), a split of tensor $\boldsymbol{\sigma}$ is also implicit in our model, and equation (3) could be expressed as

$$\psi = \frac{1}{2}\,\boldsymbol{\sigma}^{+} : \boldsymbol{D}_0^{-1} : \overline{\boldsymbol{\sigma}} + \frac{1}{2}\,\boldsymbol{\sigma}^{-} : \boldsymbol{D}_0^{-1} : \overline{\boldsymbol{\sigma}} \tag{64}$$

Therefore, the difference between the two models is evident comparing equations (63) and (64). This crucial modification does rather distinguish both models, and leads to significant computational advantages for the model here proposed, as already pointed out.

In Reference 14 a split concerning the Cauchy stress tensor is also invoked, but further complexities are included in the formulation due to the addition of a third

---

[†] Under the authors' viewpoint one should not necessarily intend to directly introduce into the local model the observed macroscopic cracking directions, since those directions should be 'better' understood as

damage variable $\tilde{d}$, linked to a coupling term describing the effects of concrete micropores:

$$\psi = \frac{\boldsymbol{\sigma}^{+} : \boldsymbol{\sigma}^{+}}{2E(1-d^{+})} + \frac{\boldsymbol{\sigma}^{-} : \boldsymbol{\sigma}^{-}}{2E(1-d^{-})} + \frac{\upsilon\,\boldsymbol{\sigma} : \boldsymbol{\sigma}\ \mathrm{tr}^{2}(\boldsymbol{\sigma})}{2E(1-\tilde{d})} \tag{65}$$

(υ is the Poisson's coefficient and tr $(\cdot)$ is the trace of tensor $(\cdot)$). Therefore an implicit formulation is also inherent to such a model, leading to great computational difficulties documented in Reference 14, namely in what concerns the stress split and the uniqueness of tensor $\boldsymbol{\sigma}$ with respect to an arbitrary strain tensor.

3.3 Equivalent strains or stresses

3.3.1 Proposed model

As observed in Figure 1, in combination with the equivalent stresses $\bar{\tau}^{\pm}$ expressed through equations (25) the damage criteria (24) encompass an elastic domain that in pure tension or in pure compression is defined by ellipsoids. This presents some advantages, since through providing a unified format for the norms and the damage criteria associated to tension and to compression the mathematical handling of the corresponding expressions becomes considerably simplified, as it became evident during the derivation of the tangent matrix. Besides, under plane stress conditions good fitting is obtained with the Kupfer *et al.*[19] envelope via such elastic stress space. Nevertheless, under 3D stress conditions the ellipsoid may be inadequate to bound the pure compressive octant, since it renders an excessively conservative envelope, like if a 'cap model' was adopted for relatively low compressive stresses. This limitation is easily circumvented by switching to another norm for the compressive stresses, as already proposed in Reference 16, where for $\bar{\tau}^{-}$ the following definition was adopted

$$\bar{\tau}^{-} = \sqrt{3}\,(K\ \bar{\sigma}^{-}_{oct} + \bar{\tau}^{-}_{oct}) \tag{66}$$

In this format, directly inspired on the Drucker-Pragger criterion, $\bar{\sigma}^{-}_{oct}$ and $\bar{\tau}^{-}_{oct}$ are the octahedral normal and shear stresses obtained from $\bar{\boldsymbol{\sigma}}^{-}$, that is,

$$\bar{\sigma}^{-}_{oct} = \mathrm{tr}(\bar{\boldsymbol{\sigma}}^{-})/3 \tag{67a}$$

---

the locus of damaged points where local instability phenomena, strain-localisation, local bifurcation and 'strong discontinuities' take place[25].

$$\bar{\tau}^{-}_{oct} = \sqrt{\bar{\boldsymbol{\sigma}}^{-} : \bar{\boldsymbol{\sigma}}^{-}/3 - \mathrm{tr}^2(\bar{\boldsymbol{\sigma}}^{-})/9} \qquad (67b)$$

K controls the aperture angle of the inherent Drucker-Pragger cone, and consequently it can be devised to fit the experimental results in the 2D compression-compression domain. Obviously under 2D plane stress conditions definition (66) performs identically to (25), leading to a bounding curve similar to the one depicted in Figure 1, but under 3D compression the open bounding surface inherent to the Drucker-Pragger cone is considered to be more suitable for concrete. The selection of any of the two definitions (equations (25) or (66)) is a matter of choice, with no particular numerical difficulties arising when implementing any of them.

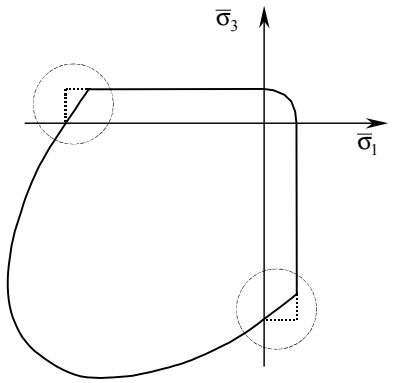

Figure 5. Reshaping the initial 2D elastic domain.

Another comment is addressed to the non-convexity of the initial 2D elastic domain depicted in Figure 1 for the model detailed in Section 2. In fact this feature is not so cumbersome as it seems, since no 'closest point projection' concept was invoked in the formulation. Anyway, it is possible to reshape such domain in order to convert it into a convex one by simply replacing $\bar{\boldsymbol{\sigma}}^{-}$ with $\bar{\boldsymbol{\sigma}}$ in definitions (25) or (66) for the equivalent stresses. It is important to remark that this change does not interfere with the proposed stress split, neither with the remnant model formulation: the split of the effective stress tensor provides the essential tool for monitoring the stress components which are to be associated to compression, but for the points located in the tension-compression corner responsible for the loss of convexity the threshold in compression is updated by using the effective stress tensor $\bar{\boldsymbol{\sigma}}$, instead of $\bar{\boldsymbol{\sigma}}^{-}$. Thermodynamic consistency of this arrangement is almost self-evident, since with reference to the standard procedure it enforces a slightly increased evolution of the

damage variable d^-. Figure 5 reproduces the new convex configuration of the reshaped elastic domain.

3.3.2 Some purely strain-based damage models

In Reference 12 an isotropic scalar damage model is presented where crack propagation is assumed to be a consequence of the development of positive straining, and accordingly an equivalent strain of the form

$$\tau_{\boldsymbol{\varepsilon}} = \sqrt{\sum_{i=1}^{3} <\varepsilon_i>^2} \tag{68}$$

is adopted, where ε_i is the *i*-th principal strain. In addition, a loading surface with the equation

$$g(\tau_{\boldsymbol{\varepsilon}}, r) = \tau_{\boldsymbol{\varepsilon}} - r \tag{69}$$

is introduced, where the hardening-softening parameter *r* retains the largest value of the equivalent strain $\tau_{\boldsymbol{\varepsilon}}$ ever reached. As for the damage variable *d*, a weighted sum of the tensile damage d^+ and the compressive damage d^- is computed as

$$d = \alpha^+ d^+ + \alpha^- d^- \tag{70}$$

where coefficients $\alpha^\pm$ depend on the tensile and compressive strain tensors $\boldsymbol{\varepsilon}^\pm$, these ones defined according to

$$\boldsymbol{\varepsilon}^+ = [\boldsymbol{D}(d)]^{-1} : \boldsymbol{\sigma}^+ \qquad\qquad \boldsymbol{\varepsilon}^- = [\boldsymbol{D}(d)]^{-1} : \boldsymbol{\sigma}^- \tag{71}$$

Obviously an implicit formulation is involved here, since $\boldsymbol{\varepsilon}^\pm$ depend on the Cauchy stress tensor and on the rank-four secant matrix $\boldsymbol{D}$, which in turn depends on the weighted damage *d*, entities which are not known *a priori*[†]. At a first glance it becomes clear that this formulation has already introduced some of the concepts assumed for the two scalar damage variables model here proposed, namely the split and the simple format of the scalar damage criterion inherent to equation (69). However, an important difference arises from the fact that in general we have replaced the strain entities by the effective stress tensor, but since $\overline{\boldsymbol{\sigma}}$ is itself a strain-based entity, our approach to the modelling of concrete behaviour stands in between the strain and the stress appraisals above referred. Besides, as pointed out in Reference 12, this version of the isotropic

[†] Concerning the specific evolution laws for $d^\pm$ and the definitions for $\alpha^\pm$, a visit to Reference 12 is

scalar damage model is unable to account for the unilateral effect, and consequently its domain of application is confined to situations in which local damages develop preferentially in mode I or in mixed I and II fracture modes. This can be also ascertained through inspection of Figure 6*a*, where the 2D elastic domain inherent to the damage criterion (69) is reproduced: it becomes clear that the compression-compression quadrant is too restrictive when compared to the one from Kupfer *et al.*[19] depicted in Figure 1.

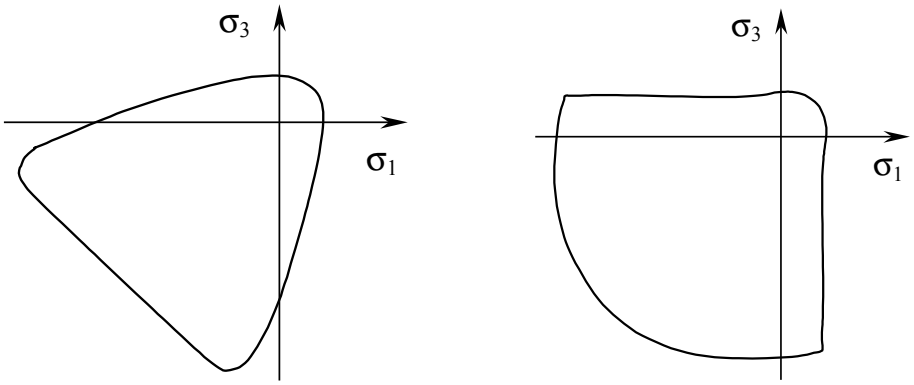

a) one scalar damage variable *b)* two scalar damage variables

Figure 6. Scalar damage models from Mazars.

In Reference 20 several equivalent strains (or stresses) were also presented. Among them, a first one with the form

$$\tau_{\boldsymbol{\varepsilon}} = \sqrt{\boldsymbol{\varepsilon} : \boldsymbol{D}_0 : \boldsymbol{\varepsilon}} = \sqrt{\overline{\boldsymbol{\sigma}} : \boldsymbol{D}_0^{-1} : \overline{\boldsymbol{\sigma}}} \tag{72}$$

is evidently a preliminary version of the norms $\overline{\tau}^{\pm}$ postulated in equation (25). This definition coincides with the energy norm of the strain tensor originally proposed in Reference 18, which through the using of the elastic constitutive tensor or the compliance one (both 'undamaged') allow the interchange between the effective stress tensor and the strain tensor documented in (72). Some variants of definition (72) were also proposed in Reference 20, basically through replacing the effective stress tensor by $\overline{\boldsymbol{\sigma}}^{+}$, or by substituting the strain tensor by $\boldsymbol{\varepsilon}^{+\,\dagger}$, or even by postulating a norm like

$$\tau_{\boldsymbol{\varepsilon}} = \left(\theta + (1-\theta)/n\right) \sqrt{\boldsymbol{\varepsilon} : \boldsymbol{D}_0 : \boldsymbol{\varepsilon}} \tag{73}$$

where n is the ratio (compressive strength)÷(tensile strength) and

---

recommended.

$$\theta = \sum_{i=1}^{3} <\overline{\sigma}_i> \Big/ \sum_{i=1}^{3} \left|\overline{\sigma}_i\right| \tag{74}$$

Anyway, from the beginning it was observed that the purely strain-based norms were inadequate to fit the concrete envelope in the compression-compression domain, as pointed out for Figure 6*a*. Such undesirable performance results from the fact that the favourable effect due to the lateral confinement in concrete samples axially compressed is compatible with some lateral expansion, a feature that can not be captured by norms like (68,72-73), since they predict $\tau_{\boldsymbol{\varepsilon}}$ to increase with the lateral expansion.

3.3.3 Unilateral damage models

Considerable advances were obtained with improved versions of the previous strain-based damage models by distinguishing the tensile damage from the compressive one, as postulated for the energy potential described in equation (63). This strategy allows accounting for the stiffness recovery effect, which as demonstrated in Reference 12 improved the constitutive model described through equations (68-72) to deal with cyclic loading.

Even with this modification, and apart from the already referred important difference concerning the stress tensors which are used to define the free energy potential, such version of the Mazars model is distinguishable from our constitutive model in the damage criteria. In fact, in that reference similar basic scalar definitions are assumed

$$\tau_{\boldsymbol{\sigma}}^{+} - r^{+} \leq 0 \qquad\qquad \tau_{\boldsymbol{\sigma}}^{-} - r^{-} \leq 0 \tag{75}$$

with the norms $\tau_{\boldsymbol{\sigma}}^{\pm}$ coinciding with the damage energy release rates, that is,

$$\tau_{\boldsymbol{\sigma}}^{\pm} = -\frac{\partial \psi}{\partial d^{\pm}} = \frac{\boldsymbol{\sigma}^{\pm} : \boldsymbol{D}_0^{-1} : \boldsymbol{\sigma}^{\pm}}{2\sqrt{1-d^{\pm}}} \tag{76}$$

Formally equations (75) are analogous to equations (24) adopted for the two scalar damage variables model here proposed, but with an essential difference concerning the definitions for the norms: in equation (76) $\tau_{\boldsymbol{\sigma}}^{\pm}$ are clearly dependent on the Cauchy stress tensor and on the damage variables, whilst in our model $\overline{\tau}^{\pm}$ are strain-based entities.

---

† This split performed similarly as in equations (2) for the effective stress tensor.

Figure 6*b* reproduces the 2D elastic domain bounded by equations (75-76), clearly an improved version of the one depicted in Figure 6*b*. In the tension-tension or tension-compression quadrants such envelope is quite similar to the one reproduced in Figure 1 for our model. Nevertheless, in the compression-compression quadrant equations (75-76) are unable to bound adequately the concrete elastic domain, namely in what concerns the prediction of an increased compressive strength under equibiaxial compression (when compared to the uniaxial one), contrarily to what occurs with the damage criteria postulated in Section 2, which provide a more realistic approximation to the Kupfer's envelope.

4. APPLICATIONS

4.1 Seismic behaviour of a R/C wall

This application concerns the numerical simulation with the model described in Section 2 of the seismic behaviour of a six-floor reinforced concrete wall, experimentally tested on a shaking table. A set of three consecutive earthquakes with peak accelerations 0.24g, 0.40g and 0.71g was prescribed to the R/C wall in an increasing intensity sequence. Even for the 0.24g earthquake significant cracking was already induced in the wall, but in order to save space the results to be presented hereafter refer only to the last 0.71g seism[†]. Figure 7 reproduces this earthquake, whereas Figure 8 details the meshes adopted for the concrete, discretized with 8-noded plane stress finite elements (0.06 m thick), as well as for the steel reinforcement, simulated via 2-noded truss elements.

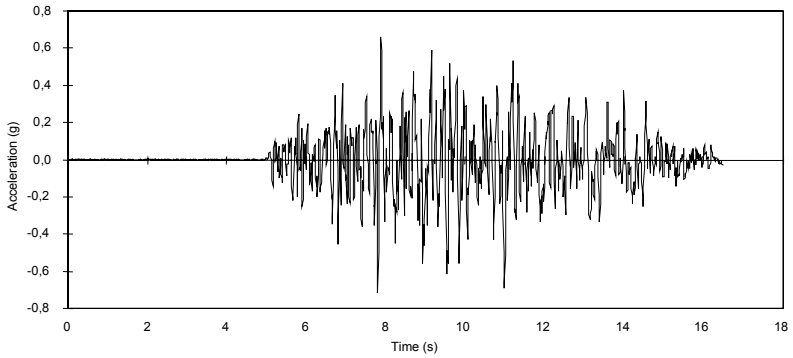

Figure 7. The 0.71g earthquake.

[†] Complimentary details may be found in Reference 26.

Three different concrete zones were considered in the wall, each of which with a particular 1D curve of the type depicted in Figure 9, and according to the properties resumed in Table 2. Zone A concerns to the concrete standing outside the stirrups (unconfined concrete), whereas B and C refer to the concrete located within the core of the stirrups existing on the lateral sides and on the centre of the wall, respectively.

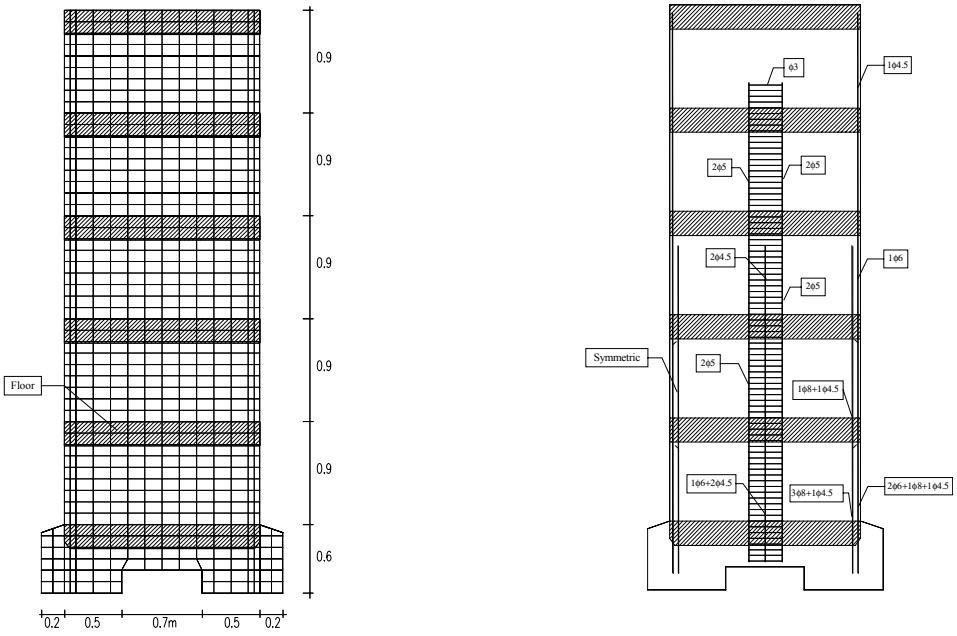

a) concrete *b)* reinforcement

Figure 8. Finite element meshes.

Table 2. Concrete properties (E = 28GPa)

Concrete	f_{co} (MPa)	ε_{co}	f_0^+ (MPa)	f_{cm} (MPa)	ε_{cm}
A	35	2‰	3.8	–	–
B	35	2‰	3.8	39.7	2.27‰
C	35	2‰	3.8	38.5	2.20‰

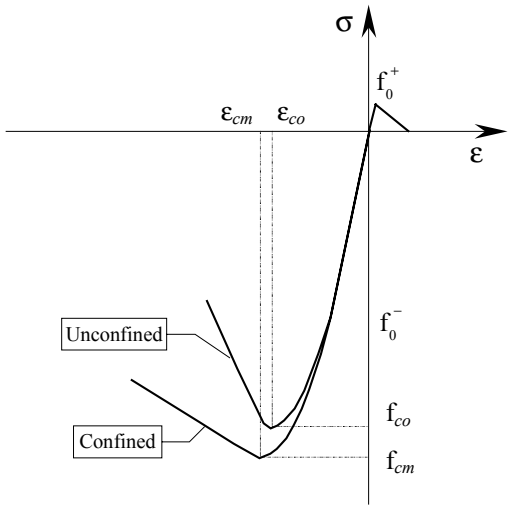

Figure 9. Confined and unconfined concrete.

Such distinction between the curves for the unconfined and the confined concrete would be unnecessary under a 3D simulation, since the constitutive model would account for the favourable effect due to the confinement provided by the stirrups. However, for the present simulation a 2D plane stress condition is being assumed, and consequently the benefits provided by the confinement along the perpendicular to the plane of representation can not be reproduced consistently by the concrete model, since a null stress condition is enforced on such direction.

Therefore we adopt here the standard procedure that consists in attributing an increased compressive strength f_{cm} to the confined concrete depending on the confinement degree k, with the latter being[27]

$$k = 1 + \frac{A_{sw}\, l_w\, f_{syt}}{b_c\, h_c\, s\, f_{co}} \tag{77}$$

where A_{sw} defines the cross sectional area of the stirrups, with perimeter l_w, separation s and yield strength f_{syt}; $b_c \times h_c$ designates the area of the concrete core effectively confined. Denoting by f_{co} and ε_{co} the compressive strength and strain for the unconfined concrete, the confinement effect may lead to the following increments on the concrete strength and peak strain (see notation in Figure 9)

$$f_{cm} = k\, f_{co} \qquad\qquad \varepsilon_{cm} = k^2\, \varepsilon_{co} \tag{78}$$

The nonlinear behaviour of the steel reinforcement was modelled with the explicit formulation due to Giuffré-Menegotto-Pinto[28]. Details concerning this standard steel

model are obviously out of scope of the present paper, but for further information the reader is addressed to References 27-28; here it suffices to say that such explicit formulation is capable of reproducing dissipative loops like the ones depicted in Figure 10.

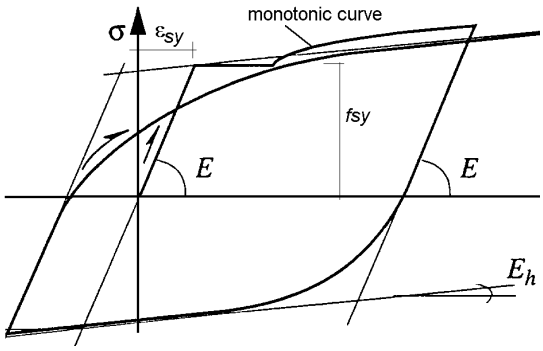

Figure 10. Steel cyclic model.

Table 3 condenses the properties assumed for the steel reinforcement layout indicated in Figure 8*b* (f_{su} and ε_{su} are the ultimate stress and strain on the monotonic curve for each steel bar, and E_h denotes the hardening modulus reproduced in Figure 10).

Table 3. Steel properties (E = 200GPa)

	ε_{sy}	ε_{su}	E_h (GPa)	f_{sy} (MPa)	f_{su} (MPa)
ϕ3	2.50‰	25‰	2.222	500	550
ϕ4.5	2.33‰	25‰	2.425	465	520
ϕ5	2.85‰	25‰	1.580	570	605
ϕ6	2.58‰	55‰	0.953	515	565
ϕ8	2.15‰	50‰	0.418	430	450

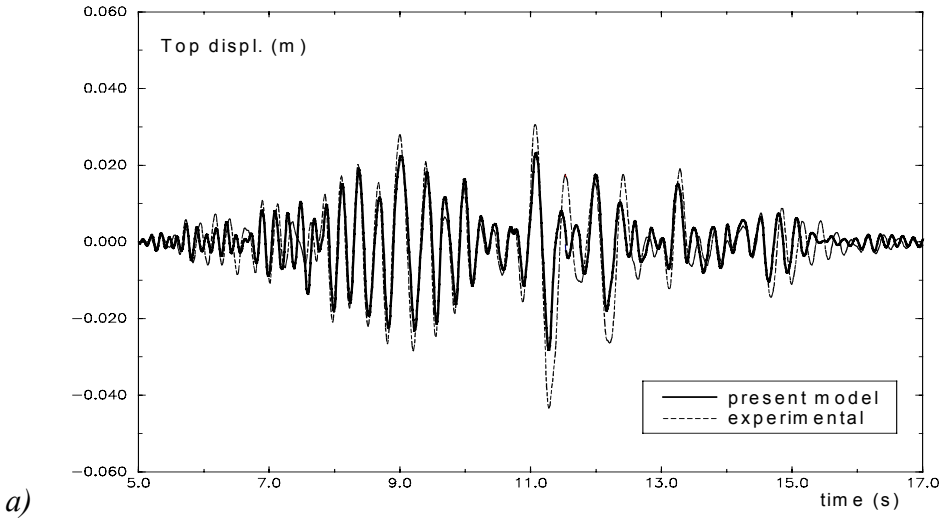

a)

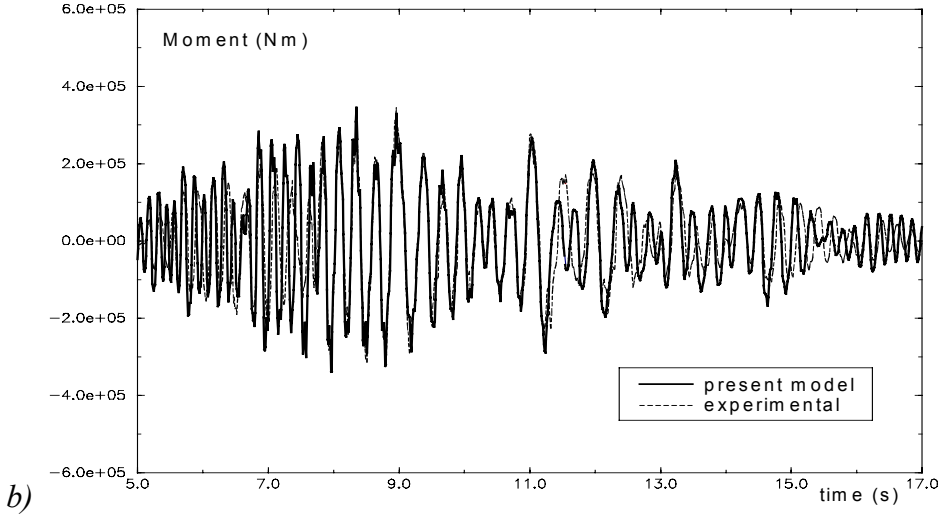

b)

Figure 11. Results after the 0.71g earthquake.

The numerical predictions from the proposed model are compared with the experimental ones in Figure 11: *(i)* in Figure 11*a* for the relative horizontal displacement registered on the top of the wall and *(ii)* in Figure 11*b* for the bending moment on the wall's footing. A good overall agreement between the numerical and the test results was obtained, with the amplitudes, the frequencies and also the phases exhibiting perfectly acceptable deviations, particularly taking into consideration that two earthquakes were already considered before the present one. The underestimation of the top displacement evident in the numerical computations may be attributed to discrepancies between computational and test conditions, namely debonding of the steel bars and poor characterisation of the material properties.

4.2 Cyclic behaviour of a R/C bridge pier

The next application shows the numerical simulation with the model described in Section 2 of a complex experimental test of a structural element under real physical conditions. It concerns a quasi-static cyclic test of a reduced-scale bridge pier, reported in Reference 27 and depicted in Figure 12*a*. Pier's height is 8.4m, and the cross section is a $0.8\times1.6\text{m}^2$ hollowed rectangle (Figure 12*b*). As reproduced in Figure 12*b*, 28ϕ14, 12ϕ12 and 40ϕ8 diameters provide the longitudinal reinforcement, whereas ϕ5 stirrups with 0.06m spacing were used for transversal reinforcement.

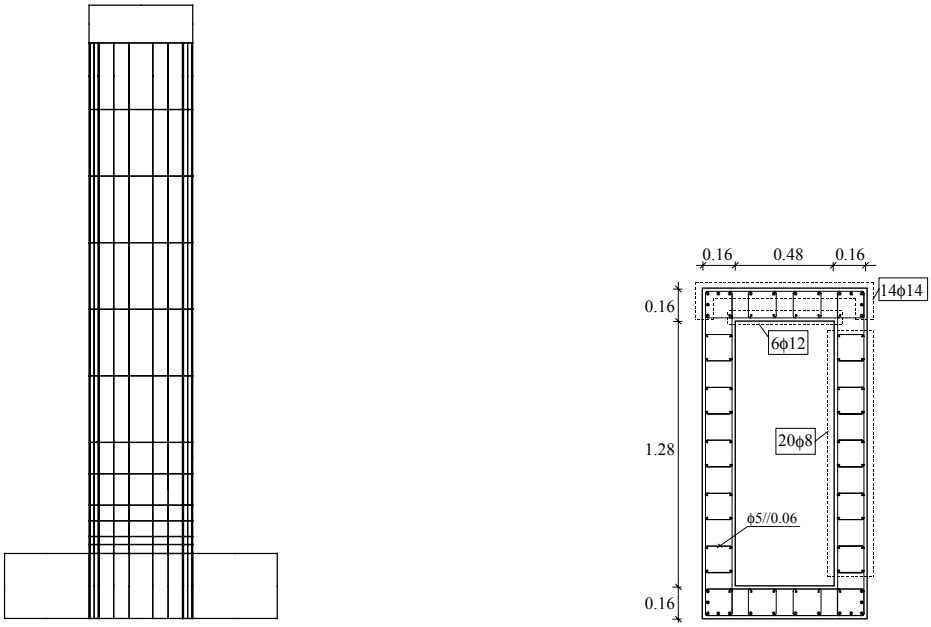

a) concrete *b)* cross section

Figure 12. R/C bridge pier.

A constant axial force of 1700kN was firstly applied to the pier's head, reproducing the vertical dead load transmitted by the deck. Afterwards a cyclic horizontal displacement was prescribed to the top of the pier, forcing it to move along the strong axis of the cross section. Owing to the geometric and load symmetries, a plane stress condition was assumed for the 8-noded finite element concrete mesh depicted in Figure 12*a*. An infinitely rigid foundation was assumed on the pier's footing.

Concerning to the material characterisation, two types of concrete were considered: *(i)* the unconfined one, which recovers the steel bars and *(ii)* the confined one, interior to the stirrups. With reference to the notation included in Figure 9 Table 4 condenses the

basic material properties for the characterisation of the 1D performance of these two types of concrete. Table 5 resumes the material properties assumed for the steel reinforcement.

Table 4. Concrete properties (E = 36GPa)

Concrete	f_{co} (MPa)	ε_{co}	f_0^+ (MPa)	f_{cm} (MPa)	ε_{cm}
Confined	50.5	2.5‰	3.8	59.6	3.0‰
Unconfined	50.5	2.5‰	3.8	-	-

Table 5. Steel properties (E = 200GPa)

Steel	ε_{sy}	ε_{su}	E_h (GPa)	f_{sy} (MPa)	f_{su} (MPa)
Longitudinal	2.50‰	100‰	1.500	500	650
Stirrups	3.50‰	16‰	2.320	700	730

Through superposing the numerical and the experimental force-displacement diagrams obtained on the top of the pier, as reproduced in Figure 13, it becomes evident the good agreement between the model predictions with the observed response for the entire loading history. Therefore, it becomes clear that under cyclic loading the two scalar damage variables model is able to reproduce the continuous change in the structural stiffness, namely the cracking of concrete, the 'pinching' effect dictated by the crack-closing, or even the nonlinearity in compression.

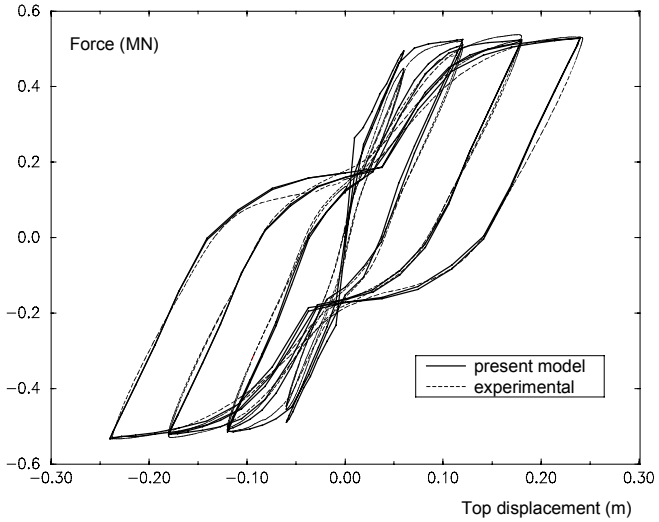

Figure 13. Force-displacement diagrams.

5. CONCLUSIONS

A constitutive model proposed by the authors and based on the Continuum Damage Mechanics is detailed. Devised for the seismic analysis of large-scale concrete structures, an effective stress tensor is selected as the basic entity for supporting the formulation. This elastic tensor is subsequently split into tensile and compressive tensor components, each of them associated to an independent scalar damage variable. With such a strategy it is possible to capture the stiffness recovery effect upon load reversal, a feature of primary importance for seismic analysis.

Owing to the strain-based formulation adopted throughout an explicit format is obtained, a particularly suitable property when dealing with large-scale problems, ensuring high algorithmic efficiency. In addition, a tangent operator is derived, an open issue in previous versions of the model due to some difficulties in expliciting time derivatives of the split stress tensors.

A comparative discussion between the proposed model and some other scalar damage ones is performed, with particular reference to the strategies pursued for introducing the split and to the norms and the damage criteria adopted in the corresponding formulations.

Finally, several numerical applications are presented, illustrating the adequacy of the constitutive model to reproduce the observed behaviour of reinforced concrete structures under cyclic motion, and consequently load reversal.

ACKNOWLEDGEMENTS

Research partially supported by the Training and Mobility of Researchers Programme, Access to Large Installations, under contract ERBFMGECT950062 “Access to supercomputing facilities for european researchers” established between The European Community and CESCA-CEPBA.

APPENDIX: DERIVATION OF OPERATOR P SUCH THAT $\dot{\bar{\boldsymbol{\sigma}}}^{+} = \mathbf{P} : \dot{\bar{\boldsymbol{\sigma}}}$

During the derivation of the tangent matrix associated to the constitutive model described in Section 2 the definition of an operator $\mathbf{P}$ such that

$$\dot{\bar{\boldsymbol{\sigma}}}^{+} = \mathbf{P} : \dot{\bar{\boldsymbol{\sigma}}} \tag{A.1}$$

was required.

Taking into consideration the definition for the tensile effective stress tensor $\overline{\boldsymbol{\sigma}}^{+}$, which can also be written as

$$\overline{\boldsymbol{\sigma}}^{+} = \sum_{i} H_i \, \overline{\sigma}_i \, \boldsymbol{p}_i \otimes \boldsymbol{p}_i \tag{A.2}$$

where $H_i = H(\overline{\sigma}_i)$ denotes the Heaviside function computed for the *i*-th principal stress $\overline{\sigma}_i$, performing a differentiation it becomes evident that

$$d\overline{\boldsymbol{\sigma}}^{+} = \sum_{i} \left[H_i \left(\boldsymbol{p}_i \otimes \boldsymbol{p}_i \right) d\overline{\sigma}_i \right] + \sum_{i} \left[H_i \, \overline{\sigma}_i \, d\left(\boldsymbol{p}_i \otimes \boldsymbol{p}_i \right) \right] \tag{A.3}$$

In subsequent steps entities $d\overline{\sigma}_i$ and $d\left(\boldsymbol{p}_i \otimes \boldsymbol{p}_i \right)$ will be explicited taking into consideration the following properties, concerning the eigenvalues and the eigenvectors of tensor $\overline{\boldsymbol{\sigma}}$:

$$\overline{\boldsymbol{\sigma}} \cdot \boldsymbol{p}_i = \overline{\sigma}_i \, \boldsymbol{p}_i \tag{A.4a}$$

$$\boldsymbol{p}_i \cdot \overline{\boldsymbol{\sigma}} \cdot \boldsymbol{p}_i = \overline{\sigma}_i \tag{A.4b}$$

$$\boldsymbol{p}_j \cdot \boldsymbol{p}_i = 0 \qquad (\text{for } j \neq i) \tag{A.4c}$$

$$\boldsymbol{p}_i \cdot \boldsymbol{p}_i = 1 \tag{A.4d}$$

- *Clarification of* $d\overline{\sigma}_i$

By differentiating equations (A.4*b*,*d*) one obtains:

$$d\overline{\sigma}_i = \boldsymbol{p}_i \cdot d\overline{\boldsymbol{\sigma}} \cdot \boldsymbol{p}_i + 2 \, d\boldsymbol{p}_i \cdot \overline{\boldsymbol{\sigma}} \cdot \boldsymbol{p}_i \tag{A.5}$$

$$d\left(\boldsymbol{p}_i \cdot \boldsymbol{p}_i \right) = 0 = 2 \, d\boldsymbol{p}_i \cdot \boldsymbol{p}_i \qquad d\boldsymbol{p}_i \cdot \boldsymbol{p}_i = 0 \tag{A.6}$$

Besides, multiplying equation (A.4*a*) by $d\boldsymbol{p}_i$ it results

$$d\boldsymbol{p}_i \cdot \overline{\boldsymbol{\sigma}} \cdot \boldsymbol{p}_i = \overline{\sigma}_i \, d\boldsymbol{p}_i \cdot \boldsymbol{p}_i \tag{A.7}$$

and owing to equation (A.6) it comes

$$d\boldsymbol{p}_i \cdot \overline{\boldsymbol{\sigma}} \cdot \boldsymbol{p}_i = 0 \tag{A.8}$$

Going back to equation (A.5), it is now possible to conclude that

$$d\overline{\sigma}_i = \boldsymbol{p}_i \cdot d\overline{\boldsymbol{\sigma}} \cdot \boldsymbol{p}_i \tag{A.9}$$

- *Clarification of* $d\left(\boldsymbol{p}_i \otimes \boldsymbol{p}_i \right)$

Differentiating $\boldsymbol{p}_i \otimes \boldsymbol{p}_i$ leads to

$$d\left(\boldsymbol{p}_i \otimes \boldsymbol{p}_i \right) = d\boldsymbol{p}_i \otimes \boldsymbol{p}_i + \boldsymbol{p}_i \otimes d\boldsymbol{p}_i \tag{A.10}$$

where $d\boldsymbol{p}_i$ is a basic entity, which requires clarification. Owing to the fact that the eigenvectors constitute an orthogonal referential, projection of $d\boldsymbol{p}_i$ onto direction $\boldsymbol{p}_j$ is expressible as $\left(d\boldsymbol{p}_i \cdot \boldsymbol{p}_j\right)\boldsymbol{p}_j$, which allows introducing the following definition for $d\boldsymbol{p}_i$

$$d\boldsymbol{p}_i = \sum_j \left(d\boldsymbol{p}_i \cdot \boldsymbol{p}_j\right)\boldsymbol{p}_j \tag{A.11}$$

According to (A.6) the situation $j=i$ can be eliminated from (A.11), and consequently

$$d\boldsymbol{p}_i = \sum_{j\neq i} \left(d\boldsymbol{p}_i \cdot \boldsymbol{p}_j\right)\boldsymbol{p}_j \tag{A.12}$$

On other hand, equation (A.4*a*) is equivalent to the homogeneous equation

$$\left(\overline{\boldsymbol{\sigma}} - \overline{\sigma}_i \boldsymbol{I}\right)\cdot \boldsymbol{p}_i = \boldsymbol{0} \tag{A.13}$$

which after differentiation leads to

$$\left(\overline{\boldsymbol{\sigma}} - \overline{\sigma}_i \boldsymbol{I}\right)\cdot d\boldsymbol{p}_i = \left(d\overline{\sigma}_i \boldsymbol{I} - d\overline{\boldsymbol{\sigma}}\right)\cdot \boldsymbol{p}_i \tag{A.14}$$

Result expressed in (A.9) allows also concluding that

$$\begin{aligned}\left(\overline{\boldsymbol{\sigma}} - \overline{\sigma}_i \boldsymbol{I}\right)\cdot d\boldsymbol{p}_i &= \left(\boldsymbol{p}_i \cdot d\overline{\boldsymbol{\sigma}} \cdot \boldsymbol{p}_i\right)\boldsymbol{p}_i - d\overline{\boldsymbol{\sigma}}\cdot \boldsymbol{p}_i = \\ &= \left(\boldsymbol{p}_i \otimes \boldsymbol{p}_i\right)\cdot d\overline{\boldsymbol{\sigma}}\cdot \boldsymbol{p}_i - d\overline{\boldsymbol{\sigma}}\cdot \boldsymbol{p}_i\end{aligned} \tag{A.15}$$

or, through pre-multiplication by $\boldsymbol{p}_j$ (with $j\neq i$),

$$\boldsymbol{p}_j \cdot \left(\overline{\boldsymbol{\sigma}} - \overline{\sigma}_i \boldsymbol{I}\right)\cdot d\boldsymbol{p}_i = \boldsymbol{p}_j \cdot \left(\boldsymbol{p}_i \otimes \boldsymbol{p}_i\right)\cdot d\overline{\boldsymbol{\sigma}}\cdot \boldsymbol{p}_i - \boldsymbol{p}_j \cdot d\overline{\boldsymbol{\sigma}}\cdot \boldsymbol{p}_i \tag{A.16}$$

Owing to the eigenvectors orthogonality expressed in equation (A.4*c*) first term on the second member of (A.16) cancels, therefore leading to

$$\boldsymbol{p}_j \cdot \left(\overline{\boldsymbol{\sigma}} - \overline{\sigma}_i \boldsymbol{I}\right)\cdot d\boldsymbol{p}_i = -\boldsymbol{p}_j \cdot d\overline{\boldsymbol{\sigma}}\cdot \boldsymbol{p}_i \tag{A.17}$$

Besides, first member on this equation is equivalent to

$$\begin{aligned}\boldsymbol{p}_j \cdot \left(\overline{\boldsymbol{\sigma}} - \overline{\sigma}_i \boldsymbol{I}\right)\cdot d\boldsymbol{p}_i &= \left(\boldsymbol{p}_j \cdot \overline{\boldsymbol{\sigma}} - \overline{\sigma}_i \boldsymbol{p}_j\right)\cdot d\boldsymbol{p}_i = \\ &= \left(\overline{\sigma}_j - \overline{\sigma}_i\right)\boldsymbol{p}_j \cdot d\boldsymbol{p}_i\end{aligned} \tag{A.18}$$

where property (A.4*a*) was invoked. According to equations (A.17-18) the following definition is hence extracted

$$\boldsymbol{p}_j \cdot d\boldsymbol{p}_i \;=\; \frac{1}{\overline{\sigma}_i - \overline{\sigma}_j}\; \boldsymbol{p}_j \cdot d\overline{\boldsymbol{\sigma}} \cdot \boldsymbol{p}_i \tag{A.19}$$

where for the present it was assumed that $\overline{\sigma}_i \neq \overline{\sigma}_j$. Substituting in (A.12) leads to

$$d\boldsymbol{p}_i \;=\; \sum_{j \neq i} \frac{1}{\overline{\sigma}_i - \overline{\sigma}_j} \left(\boldsymbol{p}_j \cdot d\overline{\boldsymbol{\sigma}} \cdot \boldsymbol{p}_i \right) \boldsymbol{p}_j \tag{A.20}$$

Due to the symmetry of tensor $d\overline{\boldsymbol{\sigma}}$ it is easy to conclude that the following property applies:

$$\boldsymbol{p}_j \cdot d\overline{\boldsymbol{\sigma}} \cdot \boldsymbol{p}_i \;=\; \boldsymbol{p}_i \cdot d\overline{\boldsymbol{\sigma}} \cdot \boldsymbol{p}_j \tag{A.21}$$

Besides, it also occurs that

$$\boldsymbol{p}_j \cdot d\overline{\boldsymbol{\sigma}} \cdot \boldsymbol{p}_i \;=\; \mathrm{tr}\left(\boldsymbol{p}_j \otimes \boldsymbol{p}_i \cdot d\overline{\boldsymbol{\sigma}} \right) \;=\; \mathrm{tr}\left(\boldsymbol{p}_i \otimes \boldsymbol{p}_j \cdot d\overline{\boldsymbol{\sigma}} \right) \tag{A.22}$$

result that can be used to support the ensuing definition

$$\begin{aligned} \boldsymbol{p}_j \cdot d\overline{\boldsymbol{\sigma}} \cdot \boldsymbol{p}_i \;&=\; \frac{1}{2} \left[\mathrm{tr}\left(\boldsymbol{p}_i \otimes \boldsymbol{p}_j \cdot d\overline{\boldsymbol{\sigma}} \right) \;+\; \mathrm{tr}\left(\boldsymbol{p}_j \otimes \boldsymbol{p}_i \cdot d\overline{\boldsymbol{\sigma}} \right) \right] = \\ &=\; \mathrm{tr} \left| \frac{1}{2} \left(\boldsymbol{p}_i \otimes \boldsymbol{p}_j \;+\; \boldsymbol{p}_j \otimes \boldsymbol{p}_i \right) \cdot d\overline{\boldsymbol{\sigma}} \right| = \\ &=\; \mathrm{tr}\left(\boldsymbol{P}^{ij} \;.\, d\overline{\boldsymbol{\sigma}} \right) \end{aligned} \tag{A.23}$$

where

$$\boldsymbol{P}^{ij} \;=\; \boldsymbol{P}^{ji} \;=\; \frac{1}{2} \left(\boldsymbol{p}_i \otimes \boldsymbol{p}_j \;+\; \boldsymbol{p}_j \otimes \boldsymbol{p}_i \right) \;=\; \mathrm{symm}\left(\boldsymbol{p}_i \otimes \boldsymbol{p}_j \right) \tag{A.24}$$

is a second-order symmetric matrix.

Back to equation (A.20), it is therefore possible to express $d\boldsymbol{p}_i$ according to

$$d\boldsymbol{p}_i \;=\; \sum_{j \neq i} \frac{1}{\overline{\sigma}_i - \overline{\sigma}_j}\; \mathrm{tr}\left(\boldsymbol{P}^{ij} \cdot d\overline{\boldsymbol{\sigma}} \right) \boldsymbol{p}_j \tag{A.25}$$

and consequently (A.10) may finally be explicited as:

$$d\left(\boldsymbol{p}_i \otimes \boldsymbol{p}_i \right) \;=\; 2 \sum_{j \neq i} \frac{1}{\overline{\sigma}_i - \overline{\sigma}_j}\; \mathrm{tr}\left(\boldsymbol{P}^{ij} \cdot d\overline{\boldsymbol{\sigma}} \right) \boldsymbol{P}^{ij} \tag{A.26}$$

Owing to (A.22) the following form may be attributed to equation (A.9):

$$d\overline{\sigma}_i \;=\; \mathrm{tr}\left(\boldsymbol{p}_i \otimes \boldsymbol{p}_i \cdot d\overline{\boldsymbol{\sigma}} \right) \tag{A.27}$$

Equation (A.24) allows to conclude that

$$\boldsymbol{p}_i \otimes \boldsymbol{p}_i \;=\; \boldsymbol{P}^{ii} \tag{A.28}$$

and therefore it is possible to transform (A.27) into

$$d\overline{\sigma}_i \;=\; \mathrm{tr}\left(\boldsymbol{P}^{ii} \cdot d\overline{\boldsymbol{\sigma}}\right) \tag{A.29}$$

Since $\boldsymbol{P}^{ii}$, $\boldsymbol{P}^{ij}$ and $d\overline{\boldsymbol{\sigma}}$ are second-order symmetric tensors, the following properties are observed:

$$\mathrm{tr}\left(\boldsymbol{P}^{ii} \cdot d\overline{\boldsymbol{\sigma}}\right) \;=\; \boldsymbol{P}^{ii} : d\overline{\boldsymbol{\sigma}} \tag{A.30a}$$

$$\mathrm{tr}\left(\boldsymbol{P}^{ij} \cdot d\overline{\boldsymbol{\sigma}}\right) \;=\; \boldsymbol{P}^{ij} : d\overline{\boldsymbol{\sigma}} \tag{A.30b}$$

Substituting these results in equations (A.26) and (A.29) it is possible to arrive to

$$d\left(\boldsymbol{p}_i \otimes \boldsymbol{p}_i\right) \;=\; 2 \sum_{j \neq i} \frac{\boldsymbol{P}^{ij} \otimes \boldsymbol{P}^{ij}}{\overline{\sigma}_i - \overline{\sigma}_j} : d\overline{\boldsymbol{\sigma}} \tag{A.31a}$$

$$d\overline{\sigma}_i \;=\; \boldsymbol{P}^{ii} : d\overline{\boldsymbol{\sigma}} \tag{A.31b}$$

Consequently equation (A.3) may be expressed as

$$d\overline{\boldsymbol{\sigma}}^{+} \;=\; \mathbf{P} : d\overline{\boldsymbol{\sigma}} \tag{A.32}$$

with

$$\mathbf{P} \;=\; \sum_i H_i \; \boldsymbol{P}^{ii} \otimes \boldsymbol{P}^{ii} \;+\; 2 \sum_i \sum_{j \neq i} \frac{< \overline{\sigma}_i >}{\overline{\sigma}_i - \overline{\sigma}_j} \; \boldsymbol{P}^{ij} \otimes \boldsymbol{P}^{ij} \tag{A.33}$$

Since $\boldsymbol{P}^{ij} = \boldsymbol{P}^{ji}$ this equation may also be transformed into

$$\mathbf{P} \;=\; \sum_i H_i \; \boldsymbol{P}^{ii} \otimes \boldsymbol{P}^{ii} \;+\; 2 \sum_{j \neq i} \frac{< \overline{\sigma}_i > - < \overline{\sigma}_j >}{\overline{\sigma}_i - \overline{\sigma}_j} \; \boldsymbol{P}^{ij} \otimes \boldsymbol{P}^{ij} \tag{A.34}$$

where the indices pair (i, j) is called only once on the second summation.

An important property applies in equation (A.34), concerning to the fact that

$$\lim_{\overline{\sigma}_i \to \overline{\sigma}_j} \frac{< \overline{\sigma}_i > - < \overline{\sigma}_j >}{\overline{\sigma}_i - \overline{\sigma}_j} = \begin{array}{ll} 0, & \text{if } \overline{\sigma}_i \leq 0 \\ 1, & \text{if } \overline{\sigma}_i > 0 \end{array} \tag{A.35}$$

which puts into evidence that no singularity occurs when $\overline{\sigma}_i = \overline{\sigma}_j$, and consequently limitation introduced about equation (A.19) is no longer restrictive.

REFERENCES

1. L. Kachanov, 'Time of rupture process under creep conditions', *Izvestia Akademii Nauk*, Otd Tech Nauk **8**, 26-31 (1958).

2. D. Krajcinovic and G. Fonseka, 'The continuum damage theory of brittle materials. Part 1: general theory', *ASME J. Appl. Mech.* **48**, 809-815 (1981).
3. D. Krajcinovic, 'Constitutive equations for damaging materials', *ASME J. Appl. Mech.* **50**, 355-360 (1983).
4. L. Resende and J. Martin, 'A progressive damage 'continuum' model for granular materials', *Comp. Meth. Appl. Mech. Engng.* **42**, 1-18 (1984).
5. J. Lemaitre, 'How to use damage mechanics', *Nucl. Engng. Des.* **80**, 233-245 (1984).
6. J. Lemaitre, 'Coupled elasto-plasticity and damage constitutive equations', *Comp. Meth. Appl. Mech. Engng.* **51**, 31-49 (1985).
7. J. Lemaitre, 'A continuous damage mechanics model for ductile fracture', *ASME J. Engng. Materials Tech.* **107**, 83-89 (1985).
8. L. Kachanov, *Introduction to Continuum Damage Mechanics*, Martinus Nijhoff Publishers, Dordrecht, 1986.
9. J. Chaboche, 'Continuum damage mechanics. Part I: general concepts', *ASME J. Appl. Mech.* **55**, 59-64 (1988).
10. J. Chaboche, 'Continuum damage mechanics. Part II: damage growth, crack initiation, and crack growth', *ASME J. Appl. Mech.* **55**, 65-72 (1988).
11. J. Lubliner, J. Oliver, S. Oller and E. Oñate, 'A plastic-damage model for concrete', *Int. J. Solids Structures* **25**, No.3, 299-326 (1989).
12. J. Mazars and G. Pijaudier-Cabot, 'Continuum damage theory. Application to concrete', *ASCE J. Engng. Mech.* **115**, No.2, 345-365 (1989).
13. I. Carol, E. Rizzi and K. Willam, 'A unified description of elastic degradation and damage based on a loading surface', *Int. J. Solids and Structures* **31**, 2835-2865 (1994).
14. C. La Borderie, Y. Berthaud and G. Pijaudier-Cabot, 'Crack closure effects in continuum damage mechanics. Numerical implementation', *Proc. 2nd Int. Conf. Comp. Aided Analysis Design Conc. Structures*, Zell am See, 975-986 (1990).
15. R. Faria and J. Oliver, *A Rate Dependent Plastic-Damage Constitutive Model for Large Scale Computations in Concrete Structures*, CIMNE Monograph **17**, Barcelona, Spain, 1993.

16. R. Faria, *Seismic Behaviour of Concrete Dams Evaluated via a Continuum Damage Model*, PhD Thesis, Porto University, Portugal, 1994 (in Portuguese).
17. R. Faria, J. Oliver and M. Cervera, 'A strain-based plastic viscous-damage model for massive concrete structures', *Int. J. Solids and Structures* **35**, No.14, 1533-1558 (1998).
18. J. Simo and J. Ju, 'Strain- and stress-based continuum damage models. I: Formulation', *Int. J. Solids Structures* **23**, No.7, 821-840 (1987).
19. H. Kupfer, H. Hilsdorf and H. Rusch, 'Behaviour of concrete under biaxial stresses', *J. Am. Conc. Inst.* **66**, No.8, 656-666 (1969).
20. J. Oliver, M. Cervera, S. Oller and J. Lubliner, 'Isotropic damage models and smeared crack analysis of concrete', *Proc. 2nd Int. Conf. Comp. Aided Analysis Design Conc. Structures*, Zell am See, 945-957 (1990).
21. J. Oliver, 'A consistent characteristic length for smeared cracking models', *Int. J. Num. Meth. Engng.* **28**, 461-474 (1989).
22. O.C. Zienkiewicz and R.L. Taylor, *The Finite Element Method*, 4th edn, McGraw-Hill, London, 1991.
23. M. Ortiz, 'A constitutive theory for the inelastic behaviour of concrete', *Mech. of Materials* **4**, 67-93 (1985).
24. J. Mazars, 'Damage models for concrete and their usefulness for seismic loadings', *Exper. and Num. Meth. in Earth. Eng.*, J. Donea and P.M. Jones (eds.), Brussels and Luxembourg, 199-221 (1991).
25. J. Oliver, M. Cervera and O. Manzoli, 'Strong discontinuities and continuum plasticity models: the strong discontinuity approach', *Int. J. of Plasticity* **3**, 319–351 (1999).
26. R. Faria, N. Vila Pouca and R. Delgado, 'Seismic behaviour of a R/C wall: numerical simulation and experimental validation', *Proc. IV Congreso de Métodos Numéricos en Ingeniería (CD-ROM)*, Sevilha (1999).
27. J. Guedes, *Seismic Behaviour of Reinforced Concrete Bridges. Modelling, Numerical Analysis and Experimental Assessment*, PhD Thesis, Porto University, Portugal, 1997.
28. M. Menegotto and P. Pinto, 'Method of analysis for cyclically loaded reinforced concrete plane frames including changes in geometry and non-elastic behaviour of

elements under combined normal force and bending', *IABSE Symp. Resist. Ultimate Deform. of Struct. Acted on by Well-Defined Repeated Loads, Final Report*, Lisbon (1973).